The FORUM End-to-End Simulator project: architecture and results

Luca Sgheri[1], Claudio Belotti[2], Maya Ben-Yami[3], Giovanni Bianchini[2], Bernardo Carnicero Dominguez[3], Ugo Cortesi[4], William Cossich[5], Samuele Del Bianco[4], Gianluca Di Natale[2], Tomás Guardabrazo[6], Dulce Lajas[3], Tiziano Maestri[5], Davide Magurno[5], Hilke Oetjen[3], Piera Raspollini[4], and Cristina Sgattoni[1]

[1]IAC – CNR, Via Madonna del Piano 10, 50019 Sesto Fiorentino (FI), Italy
[2]INO – CNR, Via Madonna del Piano 10, 50019 Sesto Fiorentino (FI), Italy
[3]ESA – ESTEC, Keplerlaan 1, 2201 AZ Noordwijk, The Netherlands
[4]IFAC – CNR, Via Madonna del Piano 10, 50019 Sesto Fiorentino (FI), Italy
[5]Physics and Astronomy Department, University of Bologna, Bologna, Italy
[6]DEIMOS Space S.L.U., Ronda de Pte. 19, 28760 Tres Cantos – Madrid, Spain

Correspondence: Luca Sgheri (l.sgheri@iac.cnr.it)

Abstract.

FORUM (Far-infrared Outgoing Radiation Understanding and Monitoring) will ~~flight~~ fly as the 9th ESA's Earth Explorer mission, and an End-to-End Simulator (E2ES) has been developed as a support tool for the mission selection process and the subsequent development phases. The current status of the FORUM E2ES project is presented, together with the characterization of the capabilities of a full physics retrieval code applied to FORUM data. We show how the instrument characteristics and the observed scene conditions impact on the spectrum measured by the instrument, accounting for the main sources of error related to the entire acquisition process, and the consequences on the retrieval algorithm. Both homogeneous and heterogeneous case studies are simulated in clear and cloudy conditions, validating the E2ES against two independent codes: KLIMA (clear sky) and SACR (cloudy sky). The performed tests show that the performance of the retrieval algorithm is compliant with the project requirements both in clear and cloudy conditions. The far infrared (FIR) part of the FORUM spectrum is shown to be sensitive to surface emissivity, in dry atmospheric conditions, and to cirrus clouds, resulting in improved performance of the retrieval algorithm in these conditions. The retrieval errors increase with increasing the scene heterogeneity, both in terms of surface characteristics and in terms of fractional cloud cover of the scene.

1 Introduction

FORUM (Far-infrared Outgoing Radiation Understanding and Monitoring, Palchetti et al. 2020) is a satellite mission selected in 2019 as the ninth ESA (European Space Agency) Earth Explorer. FORUM is conceived to fly in loose formation with IASI-NG (Infrared Atmospheric Sounder Interferometer - New Generation) on MetOp-SG-1A, and provide interferometric measurements in the 6.25–100 μm spectral interval encompassing the Far InfraRed (FIR) part of the spectrum (about 15-

100 μm) which is responsible for about 50% of the outgoing longwave flux (Harries et al., 2008) lost by our planet into space and it may be as large as 60% in polar regions.

Noteworthy, numerous satellite hyperspectral sounders are currently sampling the Mid InfraRed (MIR), such as AIRS (Chahine et al., 2006), IASI (Hilton et al., 2012) or CrIS (Han et al., 2013), but none of them is able to measure the Top of the Atmosphere (TOA) spectrum in the FIR. The unique contribution of the FORUM mission will allow to fill a major observational gap in the knowledge of the Earth energy budget and to study the role and the interactions among essential climate variables. The spectral characteristics of the incoming and outgoing radiation contain the fingerprints of surface, atmospheric and cloud processes such as those involving the water vapor ~~concentration, temperature profile~~and temperature profiles, ice cloud features and surface properties of polar and very dry regions. These components affect both the TOA energy budget and the energy distribution within the climate system. The outgoing longwave radiation, approximately from 100 to 2500 cm^{-1}, is strongly dependent on surface temperature and emissivity, greenhouse gases concentration and cloud properties among others.

In particular, the spectral coverage and resolution of the FORUM interferometer are suitable to study the signatures of three key components of the climate system:

- Upper Troposphere Lower Stratosphere (UTLS) Water vapor: Clough and Iacono (1995); Sinha and Harries (1995); Brindley and Harries (1998) demonstrated that most of the cooling of the atmosphere occurs in the UTLS by means of rotational transitions of the water vapor molecules at FIR wavelengths. For the same band it was noted by Amato et al. (2002) that radiance sensitivity to water vapor changes is higher than in the MIR. Ridolfi et al. (2020) demonstrated the benefit of ~~a FORUM-IASI data fusion for a synergistic retrieval~~ synergistic retrieval from simulated FORUM and IASI-NG measurements to provide improved L2 products among which UTLS water vapor profiles. ~~FORUM would thus~~ Significant results on the retrieval of water vapor vertical profile and continuum absorption have been obtained from the analysis of downwelling spectral radiances acquired in the far-infrared by the REFIR-PAD spectrometer at Dome-Concordia station in Antarctica, as reported by Palchetti et al. (2015) and Liuzzi et al. (2014). Thus, FORUM would be able to observe changes in the spectral signatures to ~~asses seasonal and longer-term~~ assess seasonal and interannual variations in UTLS water vapour and allow assessment of the underlying spectroscopy ~~(?)~~(ESA, 2019).

- Surface emissivity in polar and dry regions: Ice surface emissivity at FIR wavelengths has not been extensively validated (Chen et al., 2014) and most of the ~~study~~ studies are based on theoretical modelling rather than measurements . Feldman et al. (2014) estimated the impact on wrong assumption of the spectral emissivity values at FIR on decadal average Artic surface temperature of the order of 2 K. They also demonstrated the impact of surface emissivity on Artic-sea ice extent among others. Previous studies addressed the problem of simultaneous retrieval of surface temperature and emissivity by applying innovative physical inversion (Paul et al., 2012) and regularization (Masiello and Serio, 2013) schemes to IASI high spectral resolution radiances in the MIR. The FORUM mission will observe high-latitude scenes to retrieve a FIR surface emissivities dataset and possibly assess seasonal and inter-annual variability.

- Cirrus clouds: the role of ice clouds in regulating the climate has been recognized by many authors (e.g. Liou and Yang, 2016) despite the fact that thin ice clouds occurrence and properties ~~remains~~ remain uncertain especially in high latitude

regions. This is one of the reason because their representation in ~~GCMs~~ general circulation models still remains poor (IPCC, 2021). Recently, some authors (such as Maestri et al., 2019a; Saito et al., 2020; Di Natale et al., 2020) have shown the potentialities of exploiting FIR spectrally resolved radiances to refine ice clouds microphysical and optical properties. Maestri et al. (2019b) and Cossich et al. (2021) also showed the benefit of using FIR channels in combination with MIR ones to largely improve the performances of cloud identification and classification (i.e. between ice and liquid water phase) algorithms.

In the early stages of the mission development, an End-to-End Simulator (E2ES) has been devised as a tool for demonstrating proof-of-concept of the instruments and to evaluate the impact of instrument characteristics and scene conditions on the quality ~~(precision, accuracy)~~ of the retrieved products. The quality is measured in terms of precision (reproducibility of retrieved values with different random noise) and accuracy (difference between retrieved and true state). The E2ES is composed of a chain of modules which simulates the whole process of measurement acquisition, propagating all the main sources of discrepancies conceivable in operative conditions through to the retrieved geophysical quantities. Thus, it is a much more complex process than the simple simulation and retrieval that can be obtained by a single code (convolving a high-resolution spectrum with an estimate of the instrumental lineshape). The aim is to be able to single out each possible source of error and assessing the sensitivity on both the level 1 (L1) and level 2 (L2) products. In the future, this simulator will act as the testbed for ESA's operational Level 2 development and also provide data for testing measurements in applications.

The E2ES has been a support tool in the selection process, and the development has been extended after the selection to add some additional features. The E2ES version considered in this paper is that representative of the instrument knowledge of the so-called Phase B1, i.e. the preliminary definition phase of a space mission, which extended up to December 2020. In Section 2 we briefly describe the FORUM mission, and the main targets. In Section 3 we present the architecture of the E2ES and the various modules of the execution chain. In Section 4 we introduce the selected scenes used for testing. In Section 5 we show the validation and assessment tests. Finally, we draw the conclusions in Section 7.

2 The FORUM mission and role of the E2ES

2.1 The FORUM mission objectives

The FORUM mission will provide an innovative observation of the distribution of a large part of the OLR by including the unmeasured FIR part of the spectrum. The measurements will allow to quantitatively evaluate the contribution of the FIR in the radiation balance, with the goal of reducing uncertainties in the prediction of climate models.

The L1 products of FORUM will constitute a highly accurate global dataset of FIR spectral upwelling radiances in multiple atmospheric conditions which is currently unavailable to the scientific community. The dataset aims at providing a benchmark for the ~~evaluation of radiative routines~~ validation of radiative transfer models and with this also for radiative routines used in climate models through the use of satellite simulators ~~(?)~~(ESA, 2019). The objectives of the L1 FORUM radiance measurements ~~also include~~are: i) the ~~validatation~~ validation and refinement of the current spectroscopic properties (such as those

concerning water vapor and ~~in particular the continuum absorption~~carbon dioxide, e.g. ~~Serio et al. (2008)~~Mlawer et al. (2019)); ii) the evaluation of the level of accuracy of current radiative transfer codes such as the parametrisation of the water vapour continuum in an under-explored part of the spectrum, e.g. Serio et al. (2008), Koroleva et al. (2021); iii) the characterization of the radiative signal in presence of high level clouds and the enhancement of the performances of the algorithms used in cirrus cloud identification from infrared measurements only. (Maestri et al., 2019b).

In addition, the L2 products, especially if used in combination with the IASI-NG measurements, shall: i) refine the retrieval of tropospheric water vapor (Ridolfi et al., 2020) and other greenhouse gases; ii) allow the derivation of ice cloud microphysical and optical properties (Maestri et al., 2019a; Saito et al., 2020) and the definition of new parametrizations for cirrus cloud radiative schemes ~~(Di Natale et al., 2020)~~(Bozzo et al., 2008; Di Natale et al., 2020; Martinazzo et al., 2021); iii) provide surface emissivity in the FIR in polar and dry regions.

2.2 FORUM requirements

The FORUM satellite combines a Fourier transform spectrometer, namely the FORUM Sounding Instrument (FSI), and a FORUM Embedded Imager (FEI). The FEI measures a ~~a~~ radiance signal over a single band for a rectangular grid of 60 x 60 points, with a sampling step of 600 m. The FSI measures the 100–1600 cm^{-1} spectrum, with a circular Field of View (FoV) with a diameter of 15 km. The FSI FoV is centered with respect to the FEI grid since both instruments use the same telescope. The purpose of the FEI is the detection of inhomogeneities in the instrument FoV. However, since a single radiance is measured, it is difficult to assess the cause for the inhomogeneity.

The requirements for the FORUM mission were defined from the scientific objectives of the mission in the framework of ESA project FORUMreq (see the FORUMreq final report available at: https://www.forum-ee9.eu). The complete sets of requirements for the FSI Level 1 (L1, i.e. the calibrated and geo-located radiances), Level 2 (L2, i.e. the retrieved geophysical quantities) and FEI L1 products are reported in Table 1, Table 2, Table 3, respectively. In this section, only the main specifications are discussed together with their driving scientific goals.

The FSI spectral range (100–1600 cm^{-1}) was defined to cover most (~~96.7%)~~ 95% or more, (ESA, 2019, p. 43)) of the spectrum of the Earth's infrared emission to space, with a spectral resolution of 0.5 cm^{-1} to identify the spectral signatures due to seasonal, and ~~longer-term~~ interannual variations of water vapor in the upper troposphere – lower stratosphere (UTLS) range.

The requirements on precision were defined in terms of noise equivalent spectral radiance (NESR) and were set to meet the primary research objectives of FORUM: to identify FIR features of water vapor, thin cirrus clouds and surface properties.

One of the FORUM goals is to reduce uncertainty in climate predictions. The limits selected for absolute radiometric accuracy (ARA) allow to capture typical climate feedback signals associated with changes in surface temperature or perturbations in water vapor. Importantly, the goal level of accuracy (0.1 K in 300–1100 cm^{-1}) will also allow the observations to be used, with confidence, as a benchmark against which future spectrally-resolved measurements can be compared (Wielicki et al., 2013).

Table 1. FORUM FSI requirements

FSI feature	**Goal**
FSI Spectral coverage	100–1600 cm^{-1}
FSI spectral resolution (FWHM)	0.5 cm^{-1}
FSI ARA – 3σ	<0.2 K in 200–300 cm^{-1} <0.1 K in 300–1100 cm^{-1} <0.2 K in 1100–1300 cm^{-1} <1 K elsewhere
FSI NESR	0.4 $\mathrm{mW/(m^2\ sr\ cm^{-1})}$ in 200–800 cm^{-1} <1 $\mathrm{mW/(m^2\ sr\ cm^{-1})}$ elsewhere
FSI frequency calibration	1 ppm
FSI spatial sampling	$\leq$100 km

Table 2. FORUM FSI products requirements

Product	**Uncertainty requirement**
All-sky broadband spectral flux	FORUM Level 1 FIR ~~OLR~~ outgoing longwave radiation (OLR) extended to broadband with the Level 1 from IASI-NG, consistent with independent broadband flux observations to within the radiance to flux uncertainty, with minimal bias averaged over all scenes
Water vapor profile	Vertical profiles of water vapor concentration with 15% uncertainty at 2 km vertical resolution
Surface emissivity	0.01 in the 300–600 cm^{-1} spectral range for polar region on 50 cm^{-1} spectral grid
Ice water path (IWP)	20 $\mathrm{g/m^2}$
Cloud Top Height (CTH)	1 km
Particle size diameter	20%

Requirements on L2 products are realistically obtainable performances, derived by the instrument characteristics set by FSI requirements.

120 The area covered by the FEI field of view (FoV) is designed to include the FSI pixel (a circle of 7.5 km radius) and IASI-NG co-located measurements. A spatial sampling of 0.6 km is needed to detect clouds to which the FSI is sensitive (ESA, 2020; Dinelli et al., 2020).

Table 3. FORUM FEI requirements

FEI feature	Requirement
FEI FoV	instantaneous FoV covers an area on the ground surface of 36 km x 36 km
FEI spatial sampling distance, along-track and across-track	better than 0.6 km (G) and 0.75 km (T)
FEI measurement frequency	$\geq$5/dwell time of the sounder
FEI and FSI line of sight co-alignment	Co-aligned within 0.7 mrad
FEI spectral channel	11.5 µm with 2.0 µm width (G), 10.5 µm with 1.5 µm width (T)
FEI NEdT	smaller than 0.3 K (G), 0.8 K (T) at 210 K
FEI ARA	better than 1 K (G) and 2 K (T) at 210 K

2.3 The role of the E2ES

The key feature of the E2ES is the capability to introduce and single out possible causes for the discrepancies between the true and retrieved parameters. This applies both to the L1 products, i.e. the difference between the radiation reaching the instrument and the output spectrum, but also to the L2 products, i.e. the difference between the true atmospheric state and the atmospheric components retrieved by the inversion module.

The usual way of performing L2 simulations consists in using the same code for simulating the instrumental spectrum, adding some random error to the exact values, and then retrieving the atmospheric state. In other words, errors aside, all the simulated cases could be exactly retrieved by the inversion code. In the case of the E2ES, it is possible to simulate external factors which must be definitively considered in the operative life of the instrument, and that can have an impact on the accuracy of the measurements. The main factors that can be simulated by the E2ES are:

- The instrument pointing errors;
- The lack of homogeneity in the instrument field of view;
- The errors due to the instrument hardware that are not fully represented by the Instrument Spectral Response Function (ISRF), which acts as a convolution kernel on the simulated high resolution radiances.

~~By adjusting the settings, the effect of each factor can be singled out. Unfortunately, due also to the ill conditioning of the retrieval problem,~~ Unfortunately, there is often no sensitivity in the measurements to address such fine details. Nevertheless, we are able to quantify the degradation of the results due to these external factors.

The operative L2 products are affected also by the model error. The radiative transfer is performed via a code that emulates the main mechanisms governing the diffusion of the radiance in the atmosphere. Our earth is however a much more complicated

framework, the most evident difference is that the atmosphere is a continuous system, while a discretization technique has anyway to be applied in order to be fed into a computer. However, this lack of knowledge cannot be attributed to the instrument, so that adding a further uncertainty only interferes with the assessment of the instrument concept. Thus, the same forward model has been used in the generation of the scene and in the retrieval. ~~This is equivalent to knowing perfectly how~~ In this way, we are sure that the radiative transfer ~~works~~does not introduce any bias with respect to the simulated observations.

3 E2ES architecture

The E2ES is structured as a chain of modules, each performing a particular task. Each module relies on the data produced by the previous modules. The modules of the FORUM E2ES are:

- The Geometry Module (GM) calculates the true and error affected geographical coordinates of the field of view based on satellite location and pointing.
- The Scene Generator Module (SGM) calculates the high resolution radiances reaching the instrument, using the exact geographical coordinates and the prescribed atmospheric parameters. This is considered the true state.
- The Observing System Simulator (OSS) simulates the acquisition process of the instrument. Since in the preliminary phase, two different instrument concepts were available, two different configurations reproduce the two different hard-wire instrument specifications.
- The Level 2 Module (L2M) uses the spectrum generated by the OSS and the noisy geographical coordinates to retrieve atmospheric parameters.
- The Performance Assessment Module (PAM) compares the true versus the retrieved L1 and L2 products and produces a report on the discrepancies.

The execution chain can be driven and checked from an external environment, the OpenSF structure, which is tailored for this kind of simulators. Figure 1 represents the E2ES structure with the data flow.

In the following subsections we briefly describe the purpose of the various modules and sketch the algorithms. A complete documentation may be found on the website devoted to FORUM at: https://www.forum-ee9.eu/.

3.1 Geometry Module

The Geometry Module (GM) is a C++ executable in charge of providing the geolocation and observations angles for every sample of FSI and FEI instruments. This requires computing the satellite orbit, the platform attitude, the instrument line of sight and the intersection of this line with the Earth for every epoch and instrument sample.

The GM produces two types of instrument geolocation grids annotated with the sampling time and the observation angles: error-free grids (on top of which the SGM simulates the TOA spectrum) and estimated grids (intended to feed the OSS with a geolocation that is affected by telemetry and calibration uncertainties). The GM output files are written in netCDF format.

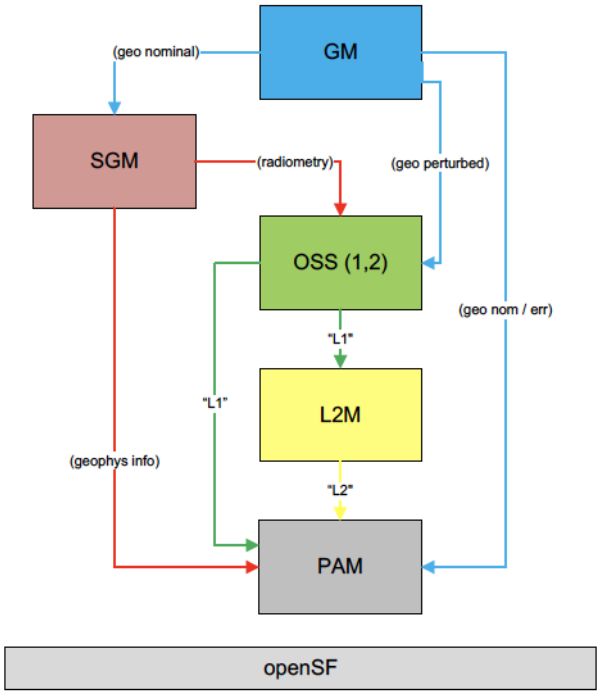

Figure 1. E2ES architecture and data flow.

The GM configuration file, which is based on XML syntax, allows the user defining several simulation parameters as the latitude and longitude of the region of interest, the acquisition start and stop times, the satellite orbit and attitude (optionally also with knowledge errors), the IERS Bulletin providing Earth Rotation Parameters, the focal length, the mirror scanning law, the focal plane arrangement of FEI and FSI instruments and the spatial oversampling factor. The line of sight modelled with these parameters for every sample is then sent to the EO-CFI (Sánchez-Nogales, 2020) for computing the geodetic coordinates of its intersection with WGS84 geoid, or the selected digital elevation model.

3.2 Scene Generator Module

The Scene Generator Module (SGM) exploits the information on geolocation and observational geometry provided by the GM and performs a simulation of gridded spectral radiances to feed the FORUM observing system simulator. The SGM computes pixel by pixel radiances, with three different approaches: a fully automatic set up, a user driven scene definition, or a mixture of the two methods.

In the automatic approach, multiple databases are loaded to configure the surface, atmosphere, and cloud properties in accordance with geolocation, season, and time of the day without any intervention from the user. For storage limit, all the databases are currently available only for observations in the range 0–85 °N and 0–30 °E, for two seasons (winter and summer),

at four times of the day (00, 06, 12, 18 UTC). The surface properties are described by the spectral emissivity, obtained from the geolocated emissivity database by Huang et al. (2016), and the skin surface temperature, obtained from the ERA 5 reanalysis data (Hersbach et al., 2020). The atmospheric profiles of temperature, pressure, water vapor, and other 11 gases mixing ratios, interpolated at fixed altitude levels, are derived from the ERA 5 reanalysis and the IG2 climatological data (Remedios et al., 2007). The gases included in the simulation are H_2O, CO_2, O_3, N_2O, CO, CH_4, O_2, NO, SO_2, NO_2, NH_3, and HNO_3. Cross section data using predefined values for the CCl_4, CFC_{11} and CFC_{12} molecules were also added. The definition of the cloud geometrical and optical properties requires multiple steps. The ERA 5 reanalysis provides the total cloud cover (cloud fraction within the pixel) and, for each vertical layer, the cloud liquid water and/or ice content (LWC and IWC). It is assumed that liquid water and ice clouds can coexist in the same layer even if they are computationally treated as two separate components. The LWC and IWC values are used to establish if the scene is clear or cloudy (total cloud cover) and for the definition of the cloud vertical structure. For each layer of the model, the liquid water particles effective radii (Re) are computed from the LWC by using the parameterization described in Martin et al. (1994), whereas the ice particle radii are derived from the IWC and the application of the parameterization by Sun and Rikus (1999) in its revised version by Sun (2001). The cloud optical depth (OD~~,~~) at 900 cm^{-1} ~~)~~ is derived, layer by layer, from ~~the information about LWC/IWC~~ information about the IWC (in case of ice clouds) or LWC (in case of liquid water clouds) and the effective ~~radii, by assuming optical properties for~~ radius of the particle size distributions ~~composed either of liquid water spheres (pre-computed) or of ice column aggregates crystals (Yang et al., 2013).~~ (PSD). The equation defining the OD at 900 cm^{-1} for vertically homogeneous clouds of geometrical thickness Δz is

$$\mathrm{OD} = \mathrm{IWC}\beta(R_{eff}, 900)\Delta z \tag{1}$$

where $\beta(R_{eff}, 900)$ is the extinction coefficient at 900 cm^{-1} of the PSD corresponding to a specific effective radius R_{eff}, normalized with respect to a unit IWC (or LWC for liquid water clouds).

Water clouds are simulated as PSDs of liquid water spheres while ice clouds are assumed as composed of 8 columns aggregates crystals. Single scattering properties for single particles (SSSP) are combined to compute the optical properties (extinction, scattering and absorption coefficients and the phase function) for a set of PSDs over the whole FORUM spectral range. The assumed PSDs are modified gamma distributions (Hansen, 1971) representatives of effective radii from 2 to 200 micrometers in case of ice clouds and from 1 to 30 micrometers in case of liquid water clouds. The SSSP are derived from Yang et al. (2013) in case of ice crystals and computed by using a Mie scattering code (Peña and Pal, 2009) when liquid water spherical particles are assumed.

Surface, atmosphere, and cloud properties are read and prepared as input for the LBLRTM (Clough et al., 2005), for clear sky description, and LBLDIS (Turner et al., 2003), for multiple scattering, cloudy sky description. These radiative transfer routines compute the spectral radiances for the FORUM imager and sounder. The default output spectral resolution is set to 10^{-2} cm^{-1} and ~~10^{-4}~~10^{-3} cm^{-1} for cloudy and clear sky simulations respectively. The different resolution is adopted for the two cases as a compromise between computational speed and accuracy. In fact, for a resolution of 10^{-2} cm^{-1} the computational times

in cloudy conditions decrease by a factor ranging from about 10 to about 20 with respect to using a 10^{-3} cm^{-1} resolution. Nevertheless, the simulation accuracy is maintained since OSS-FSI radiances in cloudy conditions computed using 10^{-2} or 10^{-3} cm^{-1} differ less than FSI goal NESR (Figure not shown).

In the user driven approach, the scene is manually configured and the user is able to set a large set of input parameters to customize the specific simulation. Basically, all the parameters defining the surface and cloud properties are user configurable. Nevertheless, the vertical atmospheric profiles are automatically selected from the ERA 5/IG2 databases for the required geolocation and data, as in the automatic approach. However, the SGM configuration parameters include the list of the atmospheric gases used for the simulation and thus, for each of them, their absorption properties can be turned off on request. The SGM allows the user to define surface temperature and emissivity, or to select specific emissivities from a list of 11 pre-defined surface types ~~(~~derived from Huang et al. 2016, e.g., water, desert, snow, deciduous vegetation~~)~~. Two different kinds of surface can be assumed to exist in the FORUM field of view. The shape of the areas covered by different surfaces (with different emissivity and temperature) are defined by sectors or circles whose sizes are set by the user through proper geometric parameters in the SGM configuration list. The scene can be assumed as clear, overcast, or partially cloudy adding a third/fourth level of possible heterogeneity to the observed scene. In this last case, the cloud covers only a fractional area of the full FORUM field of view, corresponding to a sector or a circle with configurable geometric features such as in the case of the inhomogeneous surface scene. Liquid water, ice, or mixed phase clouds can be placed at different top altitudes and be of any thickness, even overlapping each other when two clouds are assumed in the same scene (e.g. liquid-ice or ice-ice). In case of ice clouds at the moment, the user is allowed to choose between two ice particle shapes (column aggregates or hexagonal plates) whose properties are derived from Yang et al. (2013), whereas the mixed phase particles are considered to be spheres with an ice core and a liquid coating. The cloud optical properties are defined by selecting the particle size distribution effective radius and the total optical depth (at 900 cm^{-1}). All the configuration parameters are used to prepare the input files for the radiative transfer routines and to properly combine the output spectral radiances in the FORUM sounder representing the heterogenity according to the chosen spatial oversampling.

Since the setting of the surface, atmospheric, and clouds properties are independent of each other, a mixed approach can be chosen by manually configuring some components and by letting the SGM configure the others.

Once the computations are performed for each pixel of the input grid (either over-sampled to the FSI footprint or not), the synthetic spectral radiances, the input configuration parameters, and other auxiliary information are passed to the observing system simulator and to the performances assessment module.

3.3 Observing System Simulator

Just as the real instrument, the Observing System Simulator (OSS) is composed by two parallel modules, simulating the embedded imager and the Fourier interferometer.

3.3.1 FORUM Embedded Imager

The FORUM Embedded Imager Observing System Simulator (FEI-OSS) is a compiled MATLAB executable in charge of simulating and calibrating the instrument acquisition of the FEI thermal infrared imager. The FEI is modelled as an uncooled bolometer with one spectral channel centred at 10.5 μm and a 2-D sensor layout of typically 60 x 60 pixels (configurable).

The FEI OSS is composed of the instrument simulator (FEI-IS) and the L1b processor (FEI-L1).

The FEI-IS ingests the SGM output scene (possibly oversampled in the spatial domain), convolves the TOA spectra with the instrument Point Spread Function (PSF) in the spatial domain and integrates the resulting radiance with an Istrumental Spectral Response Function (ISRF) provided externally. Among its PSF modelling capabilities, the FEI-OSS is able to ingest an external PSF or to compute it by taking into account the configured parameters for the optics layout, the focal plane arrangement, the satellite motion blur and other high-frequency contributions as the AOCS jitter and the instrument micro-vibrations. Also, the channel centre is configurable.

The FEI-L1 translates the instrument output radiance into calibrated spectral radiance by taking into account noise and other instrumental errors. In particular, the noise is simulated in the brightness temperature domain with a Gaussian distribution of standard deviation equal to the configured NEdT. The calibrated radiance is finally written into the L1b product (netCDF file) along with the estimated geolocation provided by the GM module and some flags related to the FEI/FSI co-registration.

3.3.2 FORUM Sounding instrument

The FORUM Sounding Instrument Observing System Simulator (FSI-OSS) operates the software simulation of the performances of the FSI Fourier transform spectrometer from the starting point given by a set of input TOA spectral radiances provided by the Scene Generation Module (SGM). The simulator generates the interferograms corresponding to the outputs of the FSI instrument observing the selected scene, and then processes them with the level 1 data analysis code in order to recreate the observed TOA radiance.

In order to account for the effects of the finite FoV of the FSI instrument and telescope, the input radiances are provided on a sub-pixel matrix which covers the FSI footprint plus a suitable safety margin, needed to cover pointing errors in the simulations. Each of the sub-pixel is treated according to its specific observation geometry, specifically, its off-axis angle which produces a corresponding frequency shift due to the different pathlengths inside the FTS, and contributes accordingly to the output interferogram. This is the so-called self-apodisation effect.

Also, to correctly model the acquisition during the instrument dwell time, several inputs are provided to the OSS, corresponding to different times in the duration of the acquisition. Each input will have, in general, different line of sight parameters, and the result of the processing of each of the inputs is interpolated at interferogram level in order to produce the complete interferogram acquired in the duration of the dwell time.

The reference optical design used in the FSI-OSS consists in a Mach Zehnder interferometer, a design that provides the most general approach to a Fourier transform spectrometer. This design in fact allows us to place different sources on each of the two inputs of the interferometer, and different detectors on each of the two outputs. It also allows the use of separate divider

and recombiner beamsplitters, which gives greater flexibility in the instrument design. Other optical schemes can be simulated just as particular cases of this more general design.

The main configuration parameters that allow to define the interferometer performances inside the FSI-OSS are the beam splitter reflection, transmission, and absorption coefficients, which are provided as complex, spectrally-dependent quantities to obtain the most accurate and general instrument response modeling (Bianchini et al., 2009, 2019).

One of the inputs of the interferometer is permanently set on a black-body source (reference black-body, RBB), while the other can be switched between the scene and two other reference sources (cold and hot black-bodies, CBB and HBB). This allows to operate the FSI-OSS in two different modes, scene and calibration, in order to simulate the full measurement process of the FSI instrument.

To obtain a meaningful representation of the interferogram that is observed on the outputs of the FSI the OSS needs to define a further set of transfer functions that describe the behaviour of the optical and electronic components of the system.

An overall, frequency dependent absorption coefficient can be defined in order to model possible effects due to optical components. Moreover, transfer functions describing the electronics response, expressed in terms of phase and amplitude are applied in order to correctly represent the output interferograms. The electronic response function can be further subdivided into detector response and preamplifier response, if needed. A last transfer function is used to model the effects of sampling and digitization, with the possibility of introducing arbitrary random or periodic sampling errors, or a calibration error in the interferogram time scale.

All the above described functions are coded in the instrument module, which outputs the simulated interferograms. The level 1 module has the function of transforming and calibrating the interferograms in order to reconstruct the observed scene radiance (Bianchini and Palchetti, 2008). The level 1 module is subdivided in three parts:

- Level 1a, which performs the Fourier transform of the interferogram, including the possible application of compensations for the different instrumental transfer functions, the zero path difference detection and the phase correction of the interferogram, producing as output the uncalibrated spectrum.
- Level 1b, which performs the radiometric calibration of the uncalibrated spectrum and the estimation of the a-priori errors deriving from the calibration procedure (calibration error) and the detector noise (NESR error), providing as an output the measured atmospheric spectral radiance corresponding to the input scene as observed on each of the two instrument outputs.
- Level 1c, which performs the averaging of the two instrument outputs and the resampling of the average spectrum on a configurable frequency scale, in order to provide the level 2 module with a single measured spectrum with the required spectral sampling. The resampling is done through Fast Fourier Transform (FFT) interpolation and zero padding in case of oversampling.

The frequency scale is chosen to obtain statistically independent adjacent measures. This leads to a diagonal VCM matrix with respect to the NESR component, which is the dominant one. The resolutions obtained are 0.35714 and 0.37037 cm^{-1} for the two instrument concepts.

Last, a separate FSI-OSS module is used to calculate the ISRF corresponding to the configured FSI optical setup. This module performs the calculation of the ISRF taking into account the effect of the finite maximum optical path difference and the line broadening and shift due to the finite divergence of the radiation propagating inside of the interferometer (the self-apodization effect). The ISRF module generates an output file in a format which is directly compatible with the level 2 module.

3.4 Level 2 module

The L2M module is composed by the L2M_CIC (Cloud Identification and Classification) and L2M_I (Inversion) submodules. A python wrapper gathers the input data and runs the two submodules, providing the correct configuration files.

3.4.1 Cloud Identification and Classification

The main goal of the L2M_CIC submodule is to provide a classification of the observed spectrum. A machine learning algorithm named CIC (Maestri et al., 2019b) is embedded in the L2M_CIC routine and used to classify the FORUM sounder input spectrum. Four different pre-defined classes are used: clear sky, liquid water cloud, optically thick ice cloud, cirrus cloud. The classification is based on the comparison of the input spectrum with four training sets (TS), containing pre-computed spectra of the four classes. A principal component analysis determines the level of similarity of the input spectrum to the elements of each TS and selects the class of pertinence. If the spectrum is classified as cloudy (liquid water, thick ice cloud or cirrus cloud) key cloud parameters are derived and passed to the inversion module as ~~first guess~~initial conditions. The cloud parameters are: cloud top height, thickness, particle effective radius, and optical depth at 900 cm^{-1}. Their values are derived from climatological data of cloud properties (Cloud CCI: Stengel et al. 2017; cirrus clouds: Veglio and Maestri 2011) and atmospheric profiles (ERA 5: Hersbach et al. 2020), according with the cloud classification and with the geolocation, season, and observed brightness temperature at 900 cm^{-1}.

The CIC algorithm classification is based only on FORUM sounder spectral radiance and thus regards the radiance from an extended (about 15 km diameter) field of view. The classification is provided independently of the presence or not of sub-pixel heterogeneities. Therefore, a scene classified as cloudy could be the results of a field of view that is only partially covered by clouds plus a clear sky fractional area, and vice versa. The L2M_CIC exploits the FORUM imager data to pair the spectrum classification with a scene homogeneity information. The imager pixels radiances are first converted into brightness temperatures (BT), then, a BT distribution (histogram) is analysed with a custom made fitting function. A simple algorithm identifies the BT distribution modes and splits the imager pixels into homogeneous groups of pixels characterized by limited BT variation. Thus, the L2M_CIC submodule provides auxiliary information concerning the number of homogeneous areas identified at FORUM sounder sub-pixel level, their average BT and standard deviation. This is used as a quality flag for the inversion results, since non-homogeneous scenes are in any case managed as homogeneous in the retrieval process. A land mask for the imager field of view is also defined, based on the geo-referred database GSHHG (Wessel and Smith, 1996, and updates) , so that BT inhomogeneities caused by different sea-land surfaces are easily identified, especially in clear sky.

3.4.2 Inversion

The purpose of the inversion module is to solve the inverse radiative transfer problem, retrieving any combination of surface temperature, surface emissivity and vertical profiles of temperature and water vapour in clear sky conditions, and cloud parameters in cloudy sky conditions. The retrieval algorithm is based on the classical OE (Optimal Estimation) method (Rodgers, 2000). The inversion is performed via the Gauss-Newton sequence, with the Marquardt modification to ease Hessian inversion and to compensate for the non-linearity of the forward model. The a-posteriori IVS (Iterative Variable Strength) regularization technique (Ridolfi and Sgheri, 2011; Eremenko et al., 2019; Sgheri et al., 2020) is then applied to smooth out the retrieved profiles. In accordance with the SGM, the code makes use of the LBLRTM forward model in clear sky conditions, and the LBLDIS frontend to the DISORT multiple scattering code in cloudy sky conditions. ~~We used~~ In cloudy sky condition, when a cirrus cloud is detected, the inversion module includes a preprocessor that, using the parameter decoupling technique, finds a better estimate for the cloud parameters than the CIC guess. This feature is important to avoid the retrieval stopping on local minima, see the discussion of the cloudy tests for more explanations. We used the fDISORT (fast DISORT), an accelerated version of DISORT (Sgheri and Castelli, 2018), able to reduce the multiple scattering computation time. The instrumental effects are factored via the convolution with the ISRF function. In this early version of the FORUM E2ES the decision was made to maintain a frequency dependent ISRF. Consequently, the convolution cannot be computed in the Fourier domain. We obtained the actual ISRF on a rather fine grid with sampling step of 3 cm^{-1}. However, using the apodized sampled ISRF can increase the chi-square by up to 30% with respect to the unapodized spectrum, due to the fact that we exchange the interpolation and apodization operators. The correct sequence of first convolving with the sampled ISRF and then convolving with the apodization kernel increases the computation time and does not remove the error introduced by cutting the tails of the ISRF, which is one of the purposes of apodization. Thus, at least in this stage, we preferred to use the unapodized spectrum.

3.5 Performance Assessment Module

The Performance Assessment Module (PAM) is a MATLAB executable aimed to compute and plot the retrieval accuracy of L2M. In particular this module also allows inspecting the SGM output (TOA spectral radiance) and plotting the L2M vs. SGM profiles including error bars and residual statistics for clear-sky retrievals (emissivity, skin temperature, atmospheric temperature, atmospheric water vapor and precipitable water vapor) and cloudy-sky retrievals (cloud top height, cloud optical depth, cloud particle size, cloud thickness and ice/liquid water path). The PAM is also able to plot the Averaging Kernel (AK) profiles ~~computed~~ calculated by the L2M and the ~~FWHM vertical resolution(averaging~~ vertical resolution, computed at each level as the Full Width at Half Height (Rodgers, 2000) of the corresponding AK row. Averaging kernels may be optionally convolved with the SGM reference for comparison to the L2M retrievals~~)~~.

Table 4. List of homogeneous scenes considered

Case #	Scene	Geolocation	Surface	Time	Type of cloud adopted in cloudy case
1.1	Tropical	Sahara desert: 24.75°N-24.75°E	Desert	Summer	Cirrus on desert
2.1	MidLat 2	Mediterranean: 33.75°N-18.75°E	Water	Summer	Cirrus on ocean
3.1	MidLat 1	Mediterranean: 39.75°N-6.75°E	Water	Summer	Marine stratus
4.1	MidLat 3	Black forest: 50.25°N-6.75°E	Deciduous	Winter	Continental stratocumulus
5.1	Polar	Finland: 68.25°N-18.75°E	Fine snow	Winter	Ice cloud on snow ground
6.1	MidLat 4	Po Valley: 45°N,11.25°E	Deciduous	Summer	~~Cumulus nimbus~~Cumulonimbus
7.1	Polar	Kuusiluoto-Finland: 65.75°N-24.25°E	Ice	Winter	-

4 Test scenarios

The FORUM E2ES is meant to study the potentialities and criticalities of the FORUM mission for realistic characteristics of the instrument and for different measurement scenarios.

The different measurement scenarios, used both for the validation of the different modules and the assessment tests, were defined in the homogeneous case to be representative of seasons and latitudes in clear and cloudy conditions.

The FEES is able to simulate FORUM measurements all over the globe, provided the climatological data is included in the SGM dataset (see the relevant section).

Within the area selected for the ~~FEES~~ FORUM E2ES study, seven scenarios were identified: three extreme cases (two in polar regions in winter with two different surface characteristics, ice and fine snow, one in the tropics on the desert) and four cases at Middle Latitude (two on the sea, in summer, two on vegetation, one in summer and one in winter). These scenes can be simulated either in clear-sky or in cloudy-sky.

Table 4 provides, for each scene, geolocation, type of surface, and time, as well as the type of cloud assumed for each scene in the case of cloudy sky. The cloudy sky scenarios are computed adding to the clear sky atmosphere different homogeneous types of clouds filling all the FoV (see Table5).

~~While with this approximation we depart from the real data ,~~ We depart from real data using this approximation, however it does not have an impact on the assessment of the performances of the ~~FEES~~E2ES.

In the assessment tests, we also used the capability of SGM to simulate heterogeneous scenes, assuming a FoV covered by portions of different homogeneous atmospheres.

Table 5. Cloud characteristics associated to scenes considered

Case #	Cloud Type	Type	Top [km]	Thickness [km]	Total Optical Depth	Radius [μm]
1.2	Cirrus on desert	ice	12	2	1	10
2.2	Cirrus on ocean	ice	15	1	0.3	6
3.2	Marine stratus	water	1.25	0.5	20	10
4.2	Continental stratocumulus	ice	10	2	6	30
5.2	Ice cloud on snow ground	ice	8	2	3	18
6.2	~~Cumulus nimbus~~ Cumulonimbus scene	ice	11	6	300	80

5 E2ES validation and assessment tests

Assessment tests were performed to evaluate the quality of the L2 products, assuming the FORUM instruments in a configuration satisfying the L1 goal requirements, for the different scenarios identified to cover a variety of atmospheric characteristics. These tests were performed for both homogeneous and inhomogeneous scenes, in both clear sky and cloudy sky.

The results obtained in the homogeneous case represent the best that can be obtained from FORUM for the different scenes, and hence the quality of the products obtained in these conditions constitutes the reference for the other tests, performed with heterogeneous scenes.

The L2 clear sky products of the ~~E2E simulator~~ E2ES were also validated by comparing them with the outputs obtained, starting from the same observations generated by the FSI module, by an already validated correlative code. The reference code used in clear sky is KLIMA (Kyoto protocoL Informed Management of the Adaptation).

Conversely the L2 cloudy sky products of the ~~E2E simulator~~ E2ES were compared with the outputs of the reference SACR (Simultaneous Atmospheric and Cloud Retrieval) code. However, due to some differences in the model and approach, we cannot speak rigorously of a validation.

5.1 Homogeneouos Clear sky cases

The seven clear sky test case listed in Table 4 were analyzed. The simulated observed spectra were generated by the E2ES chain, including the GM, the SGM, the FEI and the FSI. The reference atmospheric state was constructed using ECMWF information. The vertical grid used to represent the atmospheric profiles in both the SGM and the L2M is composed of levels distant about 0.5 km up to 15 km, 1 km from 15 to 25 km, 5 km from 25 to 40 km, 10 km up to 80 km. In the retrieval we also tested an optimized grid similar to that of Ridolfi et al. (2020). However, in the E2ES retrieval setting we obtained worse results because a coarser grid introduces a smoothing error, particularly noticeable in the tropospheric water vapour profiles. The used noise error and spectral resolution are aligned with information provided by the industrial consortia, compliant with the goal parameters specified in Tables 1 and 3. Temperature, Water vapour, surface temperature and surface emissivity are retrieved simultaneously by L2M using the Optimal Estimation approach. The Covariance Matrices of the a-priori vertical profiles of

temperature and water vapour are built assuming the errors defined by the UK MetOffice for routine assimilation of IASI products into their operational Numerical Weather Prediction (NWP) system (see Figure 6). Indeed, IASI-NG measurements are planned to be used in synergy with the FORUM measurements. For the emissivity, which is represented on a 5 cm^{-1} spaced grid, we used a constant error of 0.05, with a correlation length in wavenumber of 50. For surface temperature an a-priori error of 2 K was used. The a-priori profiles used for these tests for all the retrieved variables are given by the truth perturbed with one standard deviation of the a-priori error. This is the most sensible choice, especially for emissivity. In fact, the sensitivity to the emissivity in the spectrum is different in different regions of the spectrum. If a stochastic perturbation were used, the results would depend on how large is the actual perturbation in the frequency ranges where there is sensitivity. For the initial condition of the retrieval we used for temperature, water vapour and surface temperature the values taken from the climatology, obtained as the 10-years local average in the month of ECMWF analysis profiles, while for emissivity the a-priori values were used. The reason for this difference is that the ~~GN~~ Gauss-Newton (GN) method only looks for local minima. Starting from the a-priori~~profiles~~, the chance to obtain a ~~profile~~ solution close to the a-priori itself ~~raises~~is not negligible. On the other hand, the dependence of the spectrum from emissivity is linear, so that the possibility of finding a local minimum for the emissivity itself is minimal. However, the combined retrieval of emissivity and surface temperature raises an issue that is discussed in this paper.

5.1.1 Validation with KLIMA code

The KLIMA code, used to validate the L2M module in clear-sky conditions, performs the retrieval of the atmospheric profiles and surface parameters from the spectral radiance measurements. The code consists of two distinct modules, the Forward Model (FM) and the Retrieval Model (RM). The RM has been developed in the context of the KLIMA ESA study (Cortesi et al., 2014) by upgrading the algorithm employed for the analysis of REFIR-PAD measurements (Bianchini et al., 2008) adapted in turn from the MARC inversion code for the MARSCHALS ESA study (Carli et al., 2007). The FM is a line-by-line radiative transfer model, with capability to simulate wideband spectral radiances, based on the following key features: radiative transfer calculations performed using Curtis–Godson approximation; atmospheric line shapes modelled with Voigt profile and atmospheric continuum model ~~takes~~ taking into account the main contributions from N_2, O_2, O_3, H_2O, and CO_2. ~~The~~ To be consistent with L2M_I, the spectroscopic database adopted for the simulations ~~are AER~~ is AER (Atmospheric and Enviromental Research) version aer_v_3.7 (http://rtweb.aer.com/line_param_frame.html), the atmospheric continuum is modelled using the routine MT_CKD_3.3 (http://rtweb.aer.com/continuum_whats_new.html) considering the contribution of the lines external to the region of ± 25 cm^{-1} from the line center. A dedicated spectroscopic database and line shape are adopted for CO_2, to take into account the line-mixing effect when using the AER ~~(Atmospheric and Enviromental Research)~~ spectroscopic database (http://rtweb.aer.com/line_param_frame.html). Moreover, the correction of the Planck function (Clough et al., 1992) is included to take into account the optical depth of the atmospheric layer at the different ~~frequency. The~~ frequencies. The only difference between the KLIMA and LBLRTM forward models is in the line-shape: KLIMA uses the Voigt function, while LBLRTM uses a linear combination of faster functions, performing a grouping of nearby lines. The validation of KLIMA FM was conducted in the context of IASI data analysis (Cortesi et al., 2014) by comparing synthetic IASI measurements gen-

Table 6. KLIMA/L2M_I retrieval quality comparison

Case #	Code	Initial reduced χ^2	Gauss iterations	Final reduced χ^2
~~1.1~~ **1.1**	KLIMA	20.46 ~~/20.45~~	3 ~~/5~~	1.07~~/~~
	L2M_I	20.45	5	1.09
~~2.1~~ **2.1**	KLIMA	2.86 ~~/2.86~~	4 ~~/~~	1.09
	L2M_I	2.86	3	1.09~~/1.09~~
~~3.1~~ **3.1**	KLIMA	4.20 ~~/4.20~~	4 ~~/~~	1.08
	L2M_I	4.20	3	1.08~~/1.08~~
~~4.1~~ **4.1**	KLIMA	2.41 ~~/2.40~~	3 ~~/3~~	1.07~~/~~
	L2M_I	2.40	3	1.08
~~5.1~~ **5.1**	KLIMA	3.66 ~~/3.65~~	3 ~~/3~~	1.07~~/~~
	L2M_I	3.65	3	1.08
~~6.1~~ **6.1**	KLIMA	3.54 ~~/~~	3	1.08
	L2M_I	3.54	3 ~~/3~~	1.08~~/1.08~~
~~7.1~~ **7.1**	KLIMA	7.19 ~~/7.19~~	9 ~~/~~	1.10
	L2M_I	7.19	4	1.10~~/1.10~~

erated by the KLIMA FM code with those of the FM of the LBLRTM. The RM uses a constrained ~~NLSF~~ non-linear least square fitting approach and the cost function to be minimized taking into account the a priori information (optimal estimation method) and the Marquardt parameter. The code implements the multi-target retrieval: more than one species is simultaneously retrieved along with many other atmospheric, surface, and instrumental parameters. A complete Covariance Matrix (CM) can be used, including both the measurement errors and the errors in the calibration procedure and/or in the estimation of the FM parameters.

The purpose of the validation was to compare the retrieved quantities and the corresponding errors (given by the mapping of measurement error on retrieved quantities) provided by the L2M~~of the E2E simulator~~ I of the E2ES and by KLIMA when starting from the same conditions. ~~From the statistical point of view the~~ The validation may be considered as reached if the differences in the estimated retrieval error ~~are negligible and differences between the retrieved values are smaller than the retrieval error. However, we also~~ and the differences in the retrieved profiles are small enough. More precisely, we set a goal at 10% of the retrieval error ~~, and we checked that, on average, the differences lie within that bound~~for the retrieved profiles. Moreover, we ask for the difference in the retrieval error to be less than 10%. With the actual results, statistically, these goals are achieved.

In Table 6 we report the comparison between the initial and final reduced χ^2 obtained using KLIMA end L2M_I. The number of Gauss iterations is also reported. Each row of the table refers to a different scenario. The Reduced χ^2 differences (both initial and final) are smaller than 0.02. Although the convergence criteria are the same (i.e. reduction of the χ^2 less than 1%), the number of Gauss iterations in some cases is different. This is due to differences on reduced χ^2 of the order of 0.001.

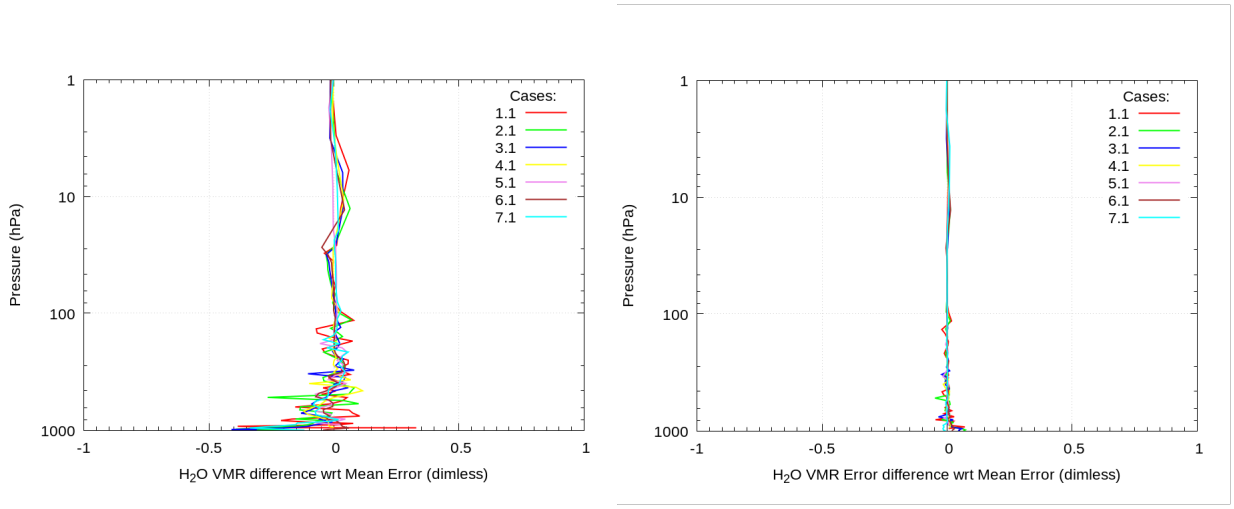

Figure 2. Left plot: Difference of the water vapour profile obtained from KLIMA and L2M_I divided the mean value of the retrieval error for the seven analysed scenarios. Right plot: Difference of the water vapour retrieval error profile obtained from KLIMA and L2M_I divided the mean value of the retrieval error for the seven analysed scenarios.

Table 7. KLIMA/L2M_I Surface Temperature Retrieval Comparison

Case #	**1.1**	**2.1**	**3.1**	**4.1**	**5.1**	**6.1**	**7.1**
KLIMA-L2M_I [K]	0.25	-0.10	0.02	0.19	-0.01	-0.05	0.03
KLIMA error [K]	0.36	0.33	0.31	0.30	0.21	0.34	0.28
L2M_I error [K]	0.34	0.34	0.31	0.30	0.21	0.34	0.27

In Figure 2 we report the comparison between the retrieved H_2O value profile and error profile obtained using KLIMA and L2M_I. The differences are divided by the mean retrieval error. The differences between retrieval errors are smaller than 5% and differences between profiles retrieved by the two codes are smaller than 0.4 times the retrieval error, with the maximal difference concentrated in the lower tropospheric region.

Results for temperature validation are reported in Figure 3. The differences between retrieval errors are smaller than 25% and the differences between profiles retrieved by the two codes are mostly smaller than 0.5 times the retrieval error.

In Table 7 we report the comparison between the retrieved surface temperature and error obtained using KLIMA and L2M_I. Each row of the table refers to a different scenario. The differences between the retrieval errors are smaller than 15% and the differences between the profiles retrieved by the two codes are mostly smaller than 0.3 times the retrieval error.

In Figure 4 we report the comparison between the spectrum of the retrieved surface emissivity and its error spectrum obtained using KLIMA and L2M_I. The differences are divided by the mean retrieval error. The differences between retrieval errors are

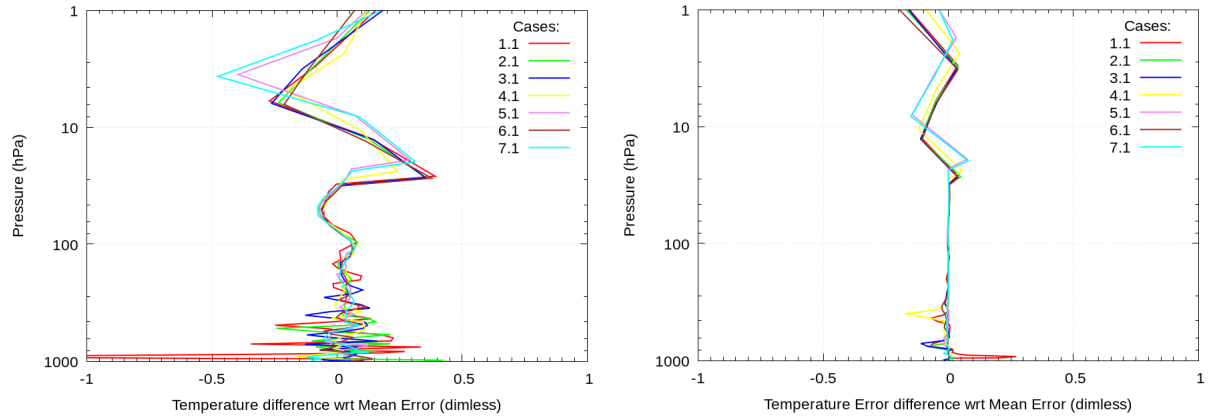

Figure 3. Left plot: Difference of the temperature profile obtained from KLIMA and L2M_I divided the mean value of the retrieval error for the seven analysed scenarios. Right plot: Difference of the temperature retrieval error profile obtained from KLIMA and L2M_I divided the mean value of the retrieval error for the seven analysed scenarios.

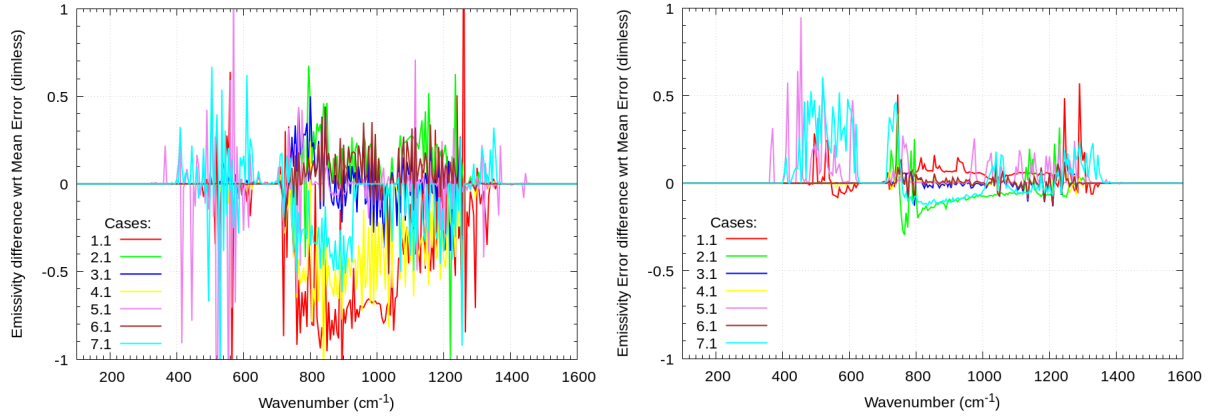

Figure 4. Left plot: Difference of the surface emissivity spectrum obtained from KLIMA and L2M_I divided the mean value of the retrieval error for the seven analysed scenarios. Right plot: Difference of the surface emissivity retrieval error spectrum obtained from KLIMA and L2M_I divided the mean value of the retrieval error for the seven analysed scenarios.

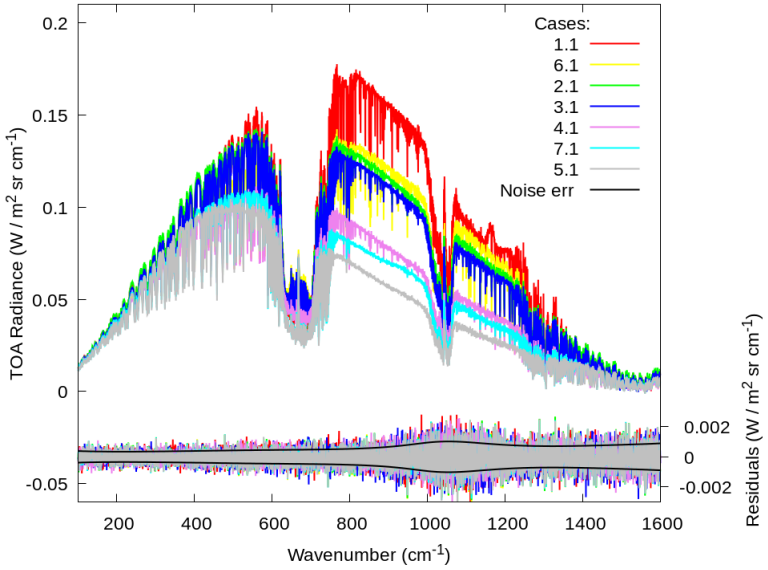

Figure 5. Simulated spectra and residuals after the fit for the seven clear cases.

smaller than 30% and the differences between profiles retrieved by the two codes are mostly smaller than 0.5 times the retrieval error. The larger differences in the MIR range that show up in some cases are mainly due to the high negative correlation between surface temperature and emissivity. For the retrieval procedure, the effect of a lower surface temperature with a higher emissivity is similar to that of a higher surface temperature with a lower emissivity.

5.1.2 Discussion of the results

We describe here a selection of the results.

In Figure 5 we report the simulated spectra and the residuals (given by the difference between simulated observations generated by the OSS and the best fit L2 simulated radiances) for the seven clear cases. The different cases are characterized by large differences both in the FIR and in the MIR spectrum. However, in all cases the residuals are compatible with the measurement noise and show no bias. In Figure 6 we report the retrieved profiles, the retrieval errors (estimated from the diagonal elements of the CM) and the differences between the retrieved and the true profiles of temperature and water vapour for all the seven cases.

For both temperature and water vapour the difference between the retrieved profile and the truth is well within the retrieval error for most of the points and all cases. Despite the variability of the temperature and water vapour profiles in the various cases, the ~~sensibility~~ sensitivity of the temperature and water vapour retrieval, given by the retrieval error, does not change significantly and the requirements on precision are met in all cases. The ~~retrieval reduces the a priori uncertainty by a factor 2 for temperatureand a factor 5~~ Information Gain Quantifier (IGQ, Dinelli et al. (2009)) is defined as two times the base 2

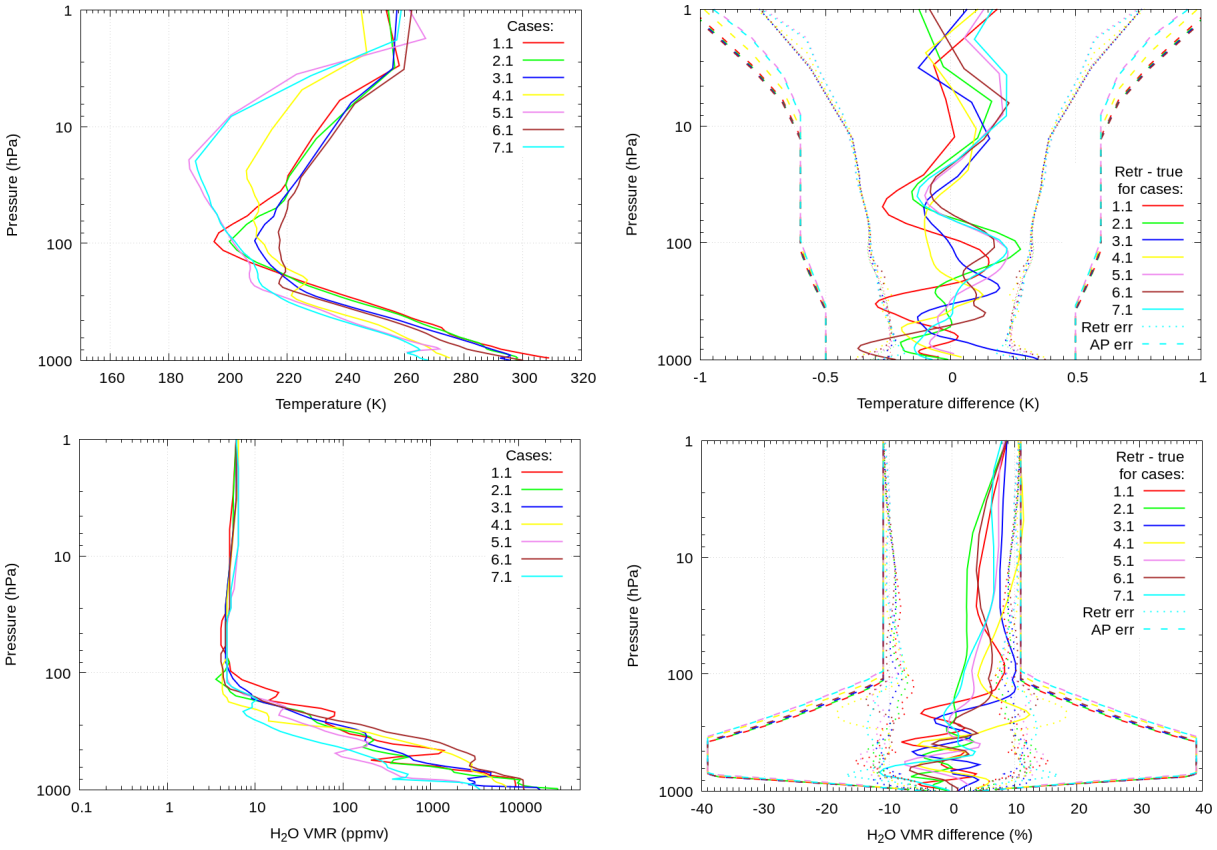

Figure 6. Retrieved temperature profiles for the seven clear sky cases (top left). Difference between retrieved and ~~associated~~ true temperature profiles, with retrieval and a-priori error (top right). Retrieved water vapor profiles for the seven clear sky cases (bottom left). Difference between retrieved and ~~associated~~ true water vapour profiles, with retrieval and a-priori error (bottom right).

logarithm of the ratio between the a-priori error and the retrieval error, and measures the contribution of the measurements in the retrieved values. The IGQ is larger than 2 for temperature, and larger than 4 for water vapour in troposphere. In Figure 7 we report the typical behaviour of the AKs for temperature and water vapour. Values of the diagonal elements significantly smaller than 1 in the troposphere does not depend only on the fact that the used a-priori errors are small and hence the information gain is limited, but also on the very fine used retrieval grid in the troposphere which determines small information content in each retrieved component. A most useful information in this case is provided by the number of degrees of freedom (DOFs), given by the trace of the averaging kernel matrix. The DOFs of the temperature profile varies from 7 for case 1.1 (tropical dry case) to about 6 for case 2.1 (middle latitude case) to 5 for ~~case5.1~~ case 5.1 (polar case), with 75% of the DOFs being concentrated in the lowest 25 km. For water vapour profile the number of DOFs varies from 8.2 for case 1.1 to 7 for case 2.1 to 5.4 for case 5.1, with more than 90% of DOFs being concentrated in the lowest 25 km. Table 8 reports the results of surface temperature retrieval. ~~While the retrieval error is smaller by at least a factor of 5 than a-priori uncertainty, all~~ All cases show a

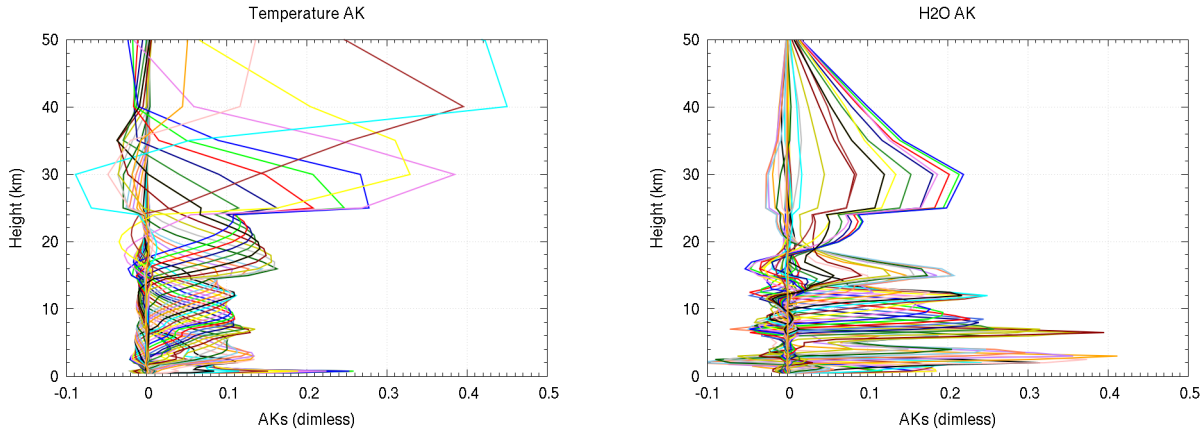

Figure 7. Averaging kernels for temperature (left panel) and water vapour (right panel) for case 1.1 (clear sky desert at noon in summer).

Table 8. Results for the retrieval of surface temperature for the seven clear sky cases.

Case #	Retrieved–True	Retrieval error	A-priori–True	A-priori error	Initial Guess–True
1.1	~~-0.815~~ –0.815	±0.34	2	±2	~~-1.333~~ –1.333
2.1	~~-0.34~~ –0.34	±0.3	2	±2	~~-0.99~~ –0.99
3.1	0.091	±0.24	2.1	±2	~~-0.073~~ –0.073
4.1	0.098	±0.279	~~-0.65~~ –0.65	±2	~~-0.436~~ –0.436
5.1	0.14	±0.21	2	±2	2.34
6.1	~~-0.224~~ –0.224	±0.393	~~-1.775~~ –1.775	±2	1.468
7.1	~~-0.073~~ –0.073	±0.23	2	±2	~~-4.9~~ –4.9

good ~~performance (differences between retrieved and true value smaller than the retrieval error)~~accuracy, with an IGQ larger than 4. The exception is case 1.1 (desert at noon in summer), where there is a negative bias of 0.8 degrees, which is larger than the retrieval error. This is due to a large negative correlation between surface temperature and emissivity in the MIR. This is further discussed when dealing with the results for surface emissivity.

For emissivity retrieval, we can divide our sample into three groups, with similar atmospheric conditions:

- The polar cases (5.1 and 7.1), high latitude and dry atmosphere (snow and ice).
- The middle latitude cases (2.1, 3.1, 4.1, 6.1), water vapour rich atmosphere over water or deciduous ground.

Table 9. Emissivity retrieval DOF for the three model cases. FIR limit is placed at 666 cm^{-1}. The retrieval grid is fixed, 301 emissivity points are retrieved, 114 belonging to the FIR and 187 to the MIR.

Case #	DOF	DOF in the FIR	DOF in the MIR
1.1	109	5	104
2.1	74	0	74
5.1	105	30	75

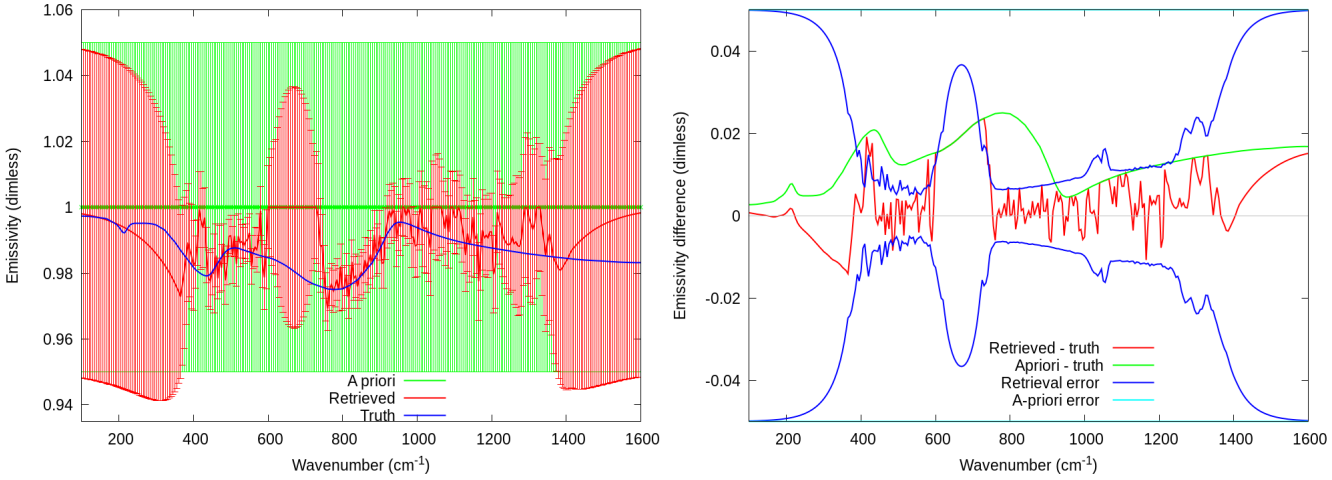

Figure 8. Emissivity retrieval for case 5.1 (polar case on fine snow). Left panel: a-priori profile with error bars (green), retrieved profile with error bars (red), truth (blue). Right panel: difference between retrieved and true (red), retrieval error (blue), difference between a-priori and model (green), a-priori error (cyan).

– The desert case (1.1), which combines a dry atmosphere and hot surface temperature. Also, the emissivity pattern has substantial features in the MIR region, the quartz Reststrahlen bands (Salisbury and D'Aria, 1992) also called the "devil's horns".

We selected one model case from each group. The number of DOF is reported in Table 9 for the FIR and MIR regions. These numbers are directly comparable because the emissivity grid is the same for all cases.

For the polar group we show case 5.1 in Figure 8. We note that, as expected due to the dry atmosphere which makes it transparent to the surface also in the FIR, there is sensitivity to the measurements both in the FIR and in the MIR regions.

This emerges also from the analysis of the AKs of the frequency dependent emissivity profile (see Figure 9), characterized by values of the diagonal matrices very close to 1 in the 500-600 cm^{-1} and in the 700-1000 cm^{-1} regions. In this regions the a-priori information contributes only very marginally to the inversion and the grid is sufficiently coarse to allow each component

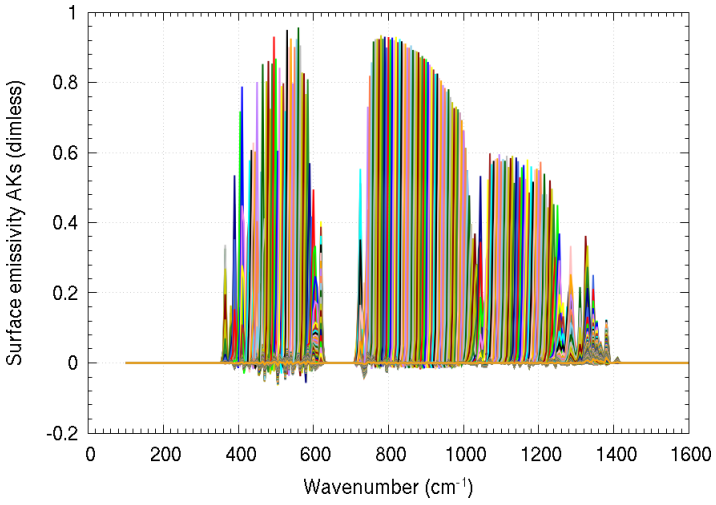

Figure 9. Averaging Kernels of the frequency dependent emissivity profile for case 5.1 (polar case on fine snow).

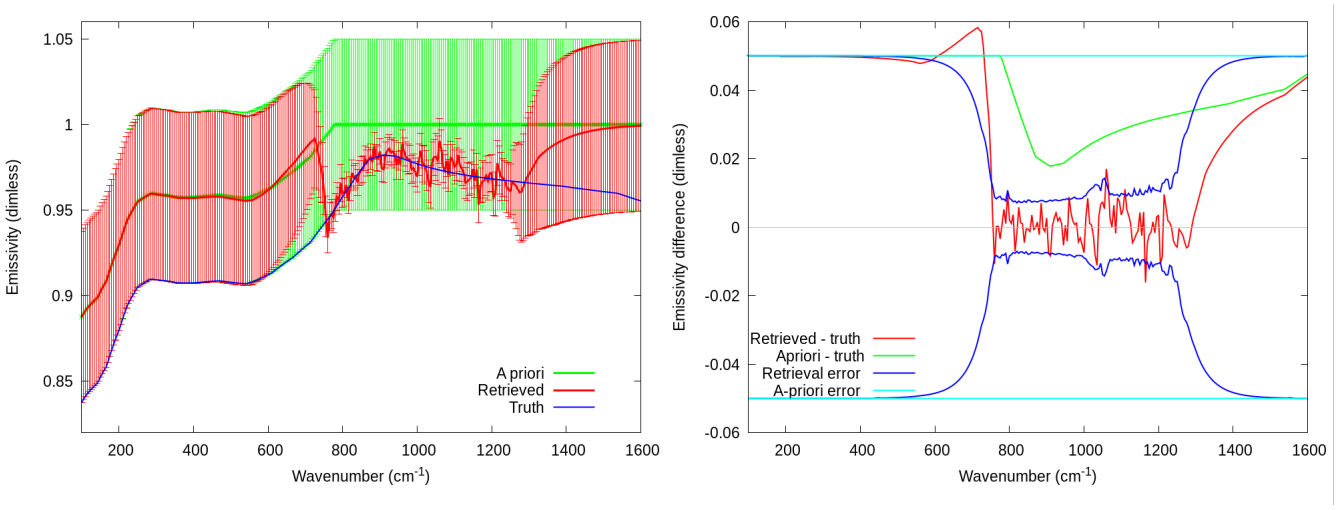

Figure 10. Emissivity retrieval for case 2.1 (middle latitude on water). Left panel: a-priori profile with error bars (green), retrieved profile with error bars (red), truth (blue). Right panel: difference between retrieved and true (red), retrieval error (blue), difference between a-priori and model (green), a-priori error (cyan).

of the used frequency grid to capture significant information. ~~The number of DOFs for the surface emissivity is 105 for the full spectral range, with the FIR spectral region contributing with 30 DOFs.~~

For the middle latitude group we show case 2.1 in Figure 10. In these cases, the rich water content in the troposphere masks the emissivity signal in the FIR, so there is only sensitivity in the MIR atmospheric window, where the transparency of the

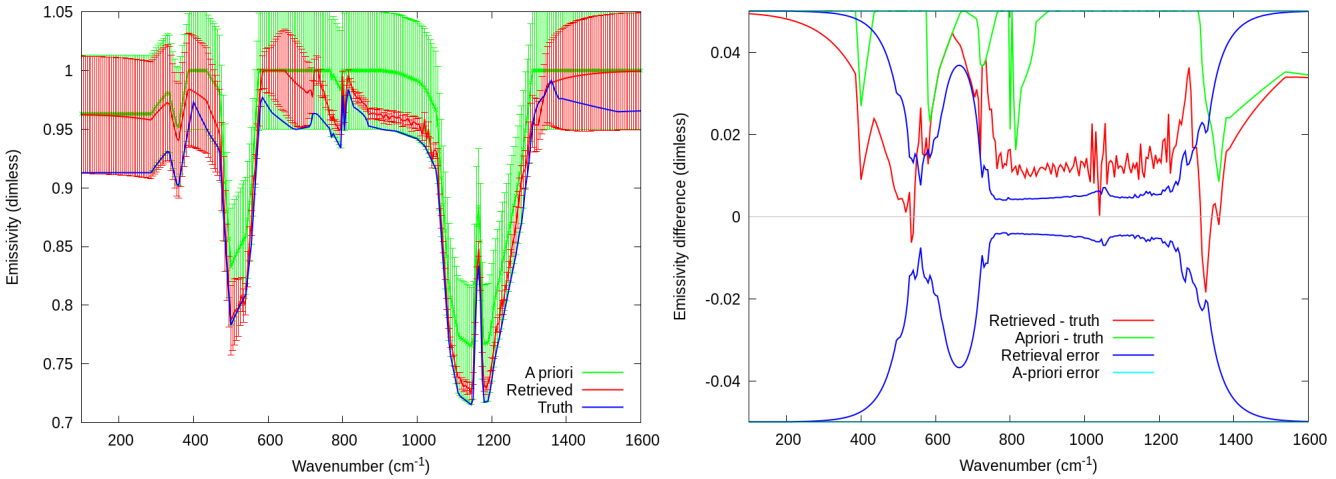

Figure 11. Emissivity retrieval for case 1.1 (desert at noon in summer). Left panel: a-priori profile with error bars (green), retrieved profile with error bars (red), truth (blue). Right panel: difference between retrieved and true (red), retrieval error (blue), difference between a-priori and model (green), a-priori error (cyan).

atmosphere allows to get information on the surface. ~~This is confirmed by the contribution to the total number of DOFs for the surface emissivity retrieval. No contribution to the DOFs comes from the FIR region, while the total number is 74.~~

Finally in case 1.1 the retrieval of the emissivity shows some sensitivity in the FIR region~~(about 5 DOFs from the FIR) on a total of 109 from the full spectral region)~~, but also a positive bias of about 0.01 in the MIR region, as shown in Figure 11.

With sensitivity tests we discovered that the bias does not depend on the particular choice of the spectrum noise. Also, the bias shows up also when retrieving only emissivity and skin temperature. The sign of the bias depends on the sign of the perturbation of the a-priori emissivity, while the initial guess of the emissivity and the initial guess and a-priori of the surface temperature have no effect. The effect is due to a strong anticorrelation between retrieved emissivity and surface temperature, which reaches ~~−0.9~~ −0.8 in the MIR region, see also right panel of Figure 13. There are different ways of solving this problem and ad-hoc studies to optimize the retrieval settings are under way. ~~A tentative solution~~ In particular, the use of a coarser emissivity grid has to be considered. One of the solutions is to use a larger a-priori emissivity error, i.e. 0.2. A larger error of the a-priori however produces oscillations in the retrieved emissivity due to the weaker constrain, which can be reduced by extending the IVS regularization to emissivity. The results are shown in Figure 12.

In Figure 13 we show the correlation matrices for the retrieved quantities in the case 1.1 (desert) and 2.1 (water). The right panel contains the correlation of the surface temperature wrt the surface emissivity in the retrieval of both cases, i.e. the rows of the leftmost columns of the two other panels corresponding to emissivity. Again we remark the strong anticorrelation between the two quantities in the retrieval, which reaches its maximum in the desert case.

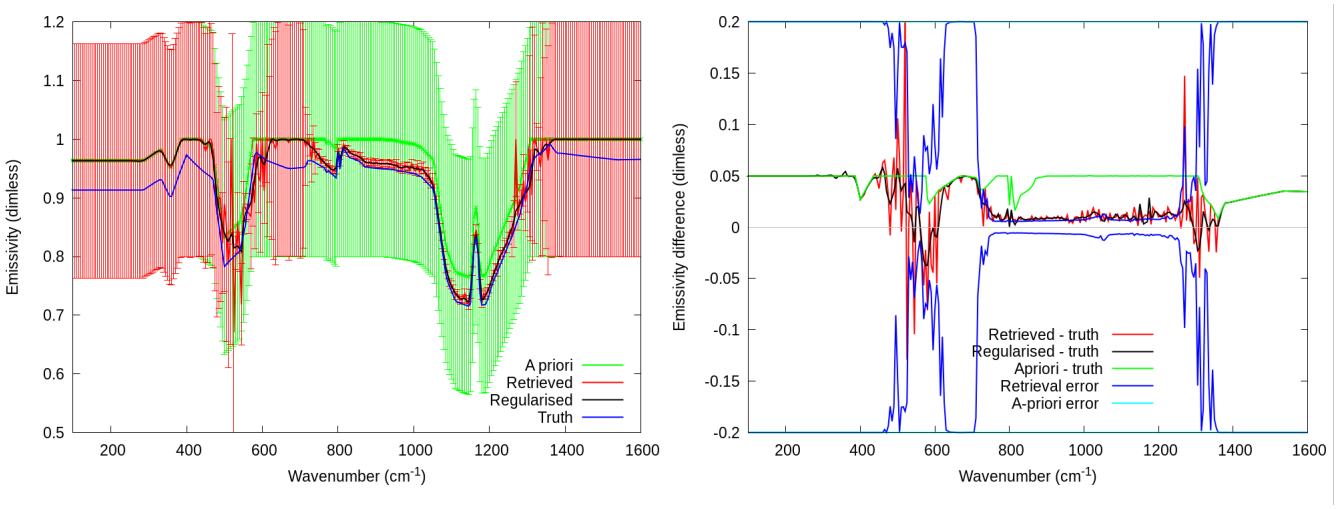

Figure 12. Emissivity retrieval for case 1.1 (desert at noon in summer). A-priori error set to 0.2 and a-posteriori regularization applied. Left panel: a-priori profile with error bars (green), retrieved profile with error bars (red), regularized retrieved profile (black), truth (blue). Right panel: difference between retrieved and true (red), retrieval error (blue), difference between regularized and model (black), difference between a-priori and model (green), a-priori error (cyan).

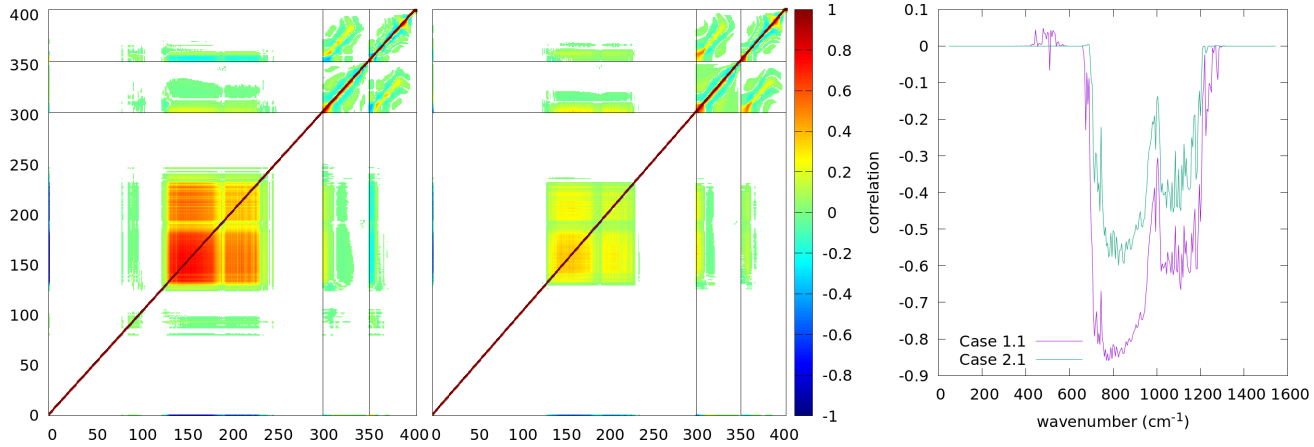

Figure 13. Correlation matrices for cases 1.1 (left panel) and 2.1 (center panel). The x and y axes represent the retrieval vector element index. Lines are drawn to separate surface temperature and emissivity sector (lower indeces), from temperature (middle indeces) and water vapour (higher indeces). Points with a positive or negative correlation less than 0.01 are not drawn to enhance the readability of the figure. In the right panel the correlation between the surface temperature and the emissivity is explicitly shown for the two cases.

5.2 Homogeneous cloudy sky cases

The second group of tests still deals with the homogeneous case, but for the cloudy-sky. The retrieval module used for the E2ES project only retrieves cloud properties in cloudy conditions. The aim of these tests is to show that, even using a perturbed atmosphere, we are still able to retrieve the cloud properties with a good precision.

The quantities retrieved in the cloudy-sky case are: the ~~altitude of the~~ top of the cloud, the equivalent radius of the particle, the total optical depth of the cloud. We realized that there is no sensitivity to the geometrical thickness of the cloud, so we assumed this parameter to be constant. The tests were performed analyzing the simulated E2ES FORUM observations related to the first six homogeneous scenarios described in Table 4 in cloudy sky condition.

5.2.1 Comparison with SACR code

The SACR code is able to perform the simultaneous retrieval of the atmospheric state and ice cloud parameters, and it was applied to the analysis of the spectral measurements acquired by the REFIR-PAD spectro-radiometer, which has been measuring at Concordia Station on the Antarctic Plateau since 2012 (Palchetti et al., 2016; Di Natale et al., 2017). The SACR code (Di Natale et al., 2020) performs the retrieval of water vapour and temperature profiles, the surface temperature, the cloud position and ~~and~~ the cloud optical and microphysical properties, such as the generalised ice and water effective diameter, the ice fraction and the optical depth or the IWP. To simulate the atmospheric radiative transfer, the LBLRTM is integrated with a specifically developed subroutine based on the δ-Eddington two-stream approximation, whereas the single-scattering properties of cirrus clouds are derived from a database for hexagonal column habits. To perform the retrieval procedure, SACR code uses the optimal estimation method with the Levenberg–Marquardt approach.

The L2 products obtained from the L2M_I and SACR are here compared. To perform a realistic validation, the atmospheric state used in the retrieval procedure is perturbed with respect to the true state according to the ~~background noise CM , and~~ CM of the a-priori. In the E2ES project, the atmospheric parameters are not retrieved. Due mainly to the differences in the cloud representation, we cannot truly speak of validation in the cloudy case. ~~Also~~In order to obtain similar results, the initial guess, a-priori and a-priori ~~conditions could not be fully replicated in the two codes, because of different code characteristics~~errors for the SACR code were taken from the output of the L2M_I preprocessor, not from the CIC estimate. The aim of the comparison is to show that the retrieval module of the E2ES and the comparative code have similar capabilities at identifying cloud properties, thus confirming that the results are not code dependent.

5.2.2 Discussion of the results

Results for five cloudy cases (the coastal marine case was wrongly attributed by the CIC to a clear sky retrieval due to the small contrast between the cloud and the surface, and case 7 was only studied in clear sky) are summarised in Table 10.

We see that, qualitatively, the results obtained by the two codes are similar. With some exceptions, the retrieved cloud parameters are very close to the true parameters, even if, being the retrieved parameters characterized by very small errors~~(given~~

Table 10. SACR/L2M_I cloudy retrieval comparison.

Cloud Top [km]	**Case 1.2**	**Case 2.2**	**Case 4.2**	**Case 5.2**	
True	12	15	10	8	
L2M_I	~~12.4~~ 11.4 ± 0.01	15.00 ± 0.05	8.77 ± ~~0.02~~ 0.05	~~8.42~~ 7.47 ± 0.01	~~15.0~~ 11.9
SACR	~~12.5~~ 11.4 ± ~~0.26~~ 0.01	~~9.40~~ 15.00 ± ~~0.03~~ ~~7.00 ±~~ 0.06	~~6.08~~ 9.59 ± 0.02	~~9.02~~ 7.38 ± ~~0.06~~0.01	1
Radius [µm]	**Case 1.2**	**Case 2.2**	**Case 4.2**	**Case 5.2**	
True	10	6	30	18	
L2M_I	10.0 ± ~~0.015~~ 0.020	~~5.86~~ 6.29 ± ~~0.02~~ 0.012	~~28.1~~ 30.9 ± ~~0.4~~ 0.2	~~17.35~~ 17.26 ± ~~0.08~~ 0.12	~~55.8~~ 63
SACR	~~10.1~~ 10.3 ± ~~0.015~~ 0.024	~~4.18~~ 6.1 ± ~~0.014~~ 0.025	~~26.3~~ 31.4 ± ~~0.4~~ 0.3	~~18.9~~ 15.2 ± ~~0.4~~ 0.18	
Optical Depth	**Case 1.2**	**Case 2.2**	**Case 4.2**	**Case 5.2**	
True	1	0.3	6	3	
L2M_I	~~0.94~~ 1.09 ± ~~0.0006~~ 0.02	~~0.297~~ 0.296 ± ~~0.0005~~ 0.001	~~5.66~~ 6.04 ± ~~0.02~~ 0.03	~~3.00~~ 2.91 ± 0.01	~~9.8~~ 8.9
SACR	~~0.99~~ 1.135 ± ~~0.0008~~ 0.001	~~0.496~~ 0.299 ± ~~0.002~~ 0.001	~~7.66~~ 6.04 ± ~~0.05~~ 0.03	~~2.88~~ 3.10 ± ~~0.01~~ 0.02	~~11.98~~ 13.0
Final chi2	**Case 1.2**	**Case 2.2**	**Case 4.2**	**Case 5.2**	
L2M_I	1.76	1.78	1.00	1.00	
SACR	2.03	1.69	1.04	1.10	

~~by square root of the diagonal elements of the Covariance Matrix of the retrieval vector)~~, in most cases, the difference between the retrieved and the true value is larger than the error.

In the ~~E2E simulations~~ E2ES the cloud composition and scattering properties are the same in the simulation and retrieval of data, so the model error, which is significant with real data and must be accounted for in the ~~Covariance Matrix~~CM, does not impact on the retrieval error.

On the other hand, there is a combination of factors that explains the small error bars:

- The error on the assumed atmosphere, which is perturbed with respect to the true state, is not taken into account in the error budget.
- The linear estimate may not be verified, especially when parameters with different ~~units are mixedin the state vector~~behavior are mixed.
- In presence of non negligible correlations in the Covariance Matrix differences between the retrieved value and the true state can be larger than the square root of the diagonal matrix. The typical absolute values of the cloud parameter correlations are in the $0.1 - 0.7$ range.

~~There are at least two cases in which the~~ The retrieval of cloud parameters ~~is critical also~~ may be critical even when cloud composition and scattering properties are ~~the same in the simulation and retrievalof data:~~ perfectly known. The following examples list the critical aspects of the retrieval.

- A water cloud at very low altitudes (case 3.2), ~~in which case the cloud~~ that is not identified because the cloud and surface effects are similar.

- ~~In the case of a cirrus cloud ,~~ A cirrus cloud combines scattered radiation from below the cloud and direct radiation from above the cloud ~~are mixed~~ in the TOA spectrum. This combination leads to the existence of local minima in the cost function which is minimised by the retrieval procedure, because different parts of the spectrum are well fitted by different cloud parameters. If the initial guess is far from the true values, the retrieval may converge to a local minimum.

  ~~For case 6.2, characterized by a very large optical depth, the retrieval values are very far from the true value. However, we verified that for thick clouds, i. e. clouds with optical depth larger than 10,~~ This problem is tackled by the ~~cloud becomes fully opaque and the sensitivity to larger optical depths~~ L2M_I by using a cloud preprocessor, as already mentioned. If the preprocessor is not used, the results of both the L2M_I and SACR for cases 1.2 and 2.2 worsen.

- A cloud characterized by a very large OD (case 6.2), where the sensitivity to the OD is lost. In this case ~~,~~ the cloud becomes fully opaque, and the only radiation seen by the instrument comes from above the cloud. ~~Indeed, for~~ The error on the spectrum using an OD=10 instead of the true value OD=300 is smaller than the requirement for the NESR, and can be seen in Figure 14.

For thick clouds, two L2M_I approximations were tested in order to reduce the ~~computing~~ computation time: maximum ~~optical depth~~ OD set to 10 and representation of the cloud as a single layer (SL) instead of multiple layers. The results are presented in Figure 14.

~~Very thick cloud case (case 6.2, optical depth larger than 100). Quantification of the error in the radiance compared with the noise requirements (yellow curve) using an optical depth of 10 when the cloud is treated either as a single layer (blue curve) or as multiple layers (green curve). The purple curve represents the error when the optical depth of 100 is used and the cloud is represented as a single layer.~~

~~The optical depth~~ The OD limit of 10, if used alone, introduces an error which is larger than the NESR, because some radiation ~~however penetrates~~ manages to penetrate the first layers of the cloud. The error ~~becomes smaller than~~ is comparable with the NESR if also the ~~single layer~~ SL approximation is applied, because the compactness of the cloud ~~avoids~~ impedes the penetration of the radiation. Indeed, ~~most of the reduction in the computation time comes from the single layer approximation alone~~the error becomes negligible if only the SL approximation is used, and the ~~effect of this optimization on the spectrum is negligible, if no limit on the optical depth is used~~speedup is stunning. The fDISORT computation time with the SL approximation is about one tenth of the computation time when no approximation is applied. On the other hand, the OD limit only subtracts some seconds. Thus, the ~~tests were performed with these settings. Of course, there is still no~~ retrievals

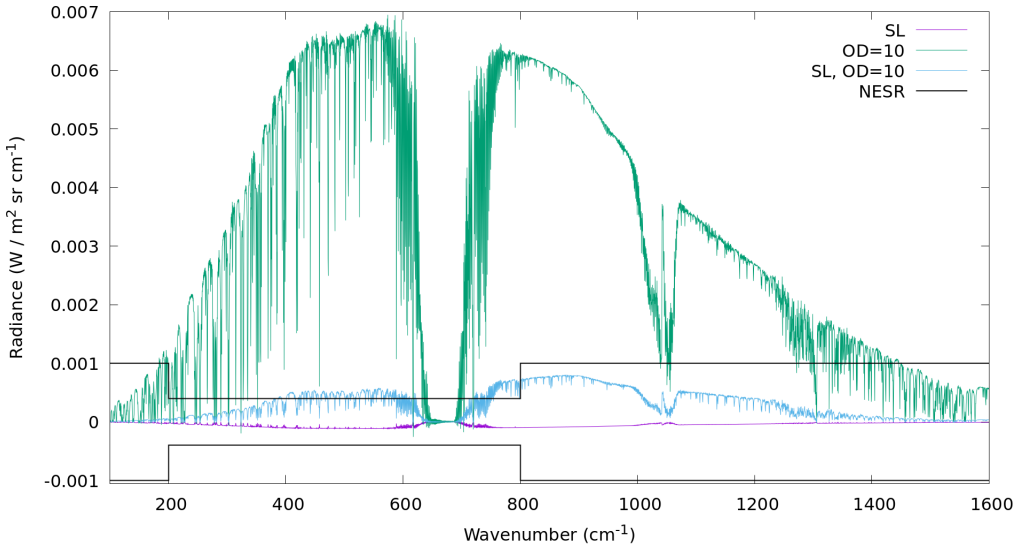

Figure 14. Very thick cloud case (case 6.2, OD=300). Quantification of the error in the radiance compared with the noise requirements (black curve) using SL approximation (purple curve), maximal OD of 10 (green curve) or both (blue curve).

were performed using the SL approximation. The drawback is that the sensitivity to large values of the ~~optical depth~~OD is even smaller, since the cloud is more compact.

5.2.3 Sensitivity to thin cirrus cloud

The far-infrared part of the spectrum is particularly sensitive to cirrus clouds and recently, simulations were used to show that FIR can contribute to improve the detection of thin cirrus cloud (Maestri et al., 2019b, a; Magurno et al., 2020). The analysis with the ~~E2E simulator~~ E2ES allows to evaluate the capability of retrieving cloud information from these measurements also in presence of very thin cirrus clouds and to compare the lowest detectable optical depth for a cirrus cloud by FORUM (range 100–1300 cm^{-1}) with the one obtainable from the analysis of Middle InfraRed (MIR) measurements only (range 667–1300 cm^{-1}). The sensitivity of the retrieval to the optical depth of the cirrus cloud depends on the contrast between the surface and the cloud and this depends on the characteristics of the surface and the atmosphere. Two cases were considered for this analysis: cirrus on the desert, and cirrus on the sea, see Table 5. The surface properties are assumed homogeneous for the entire scene.

For both cases, we started from the optical depth value of the considered case and then we progressively halved the optical depth whilst keeping all other parameters unchanged until the Cloud Identification and Classification tool continued to classify this case as cloudy. Then L2M_I retrieval was performed to be sure that the retrieval was able to retrieve the cloud parameters. Contrary to previous tests where perturbed values of the truth were used for water vapour, temperature and surface temperature,

Table 11. Cirrus cloud cases 1.2 (cirrus on desert) and 2.2 (cirrus on ocean). Minimum optical depth ~~for cirrus cloud~~ that can be detected when either all FORUM spectrum is used (FIR+MIR) or only the MIR part (667-1100 cm^{-1}) is used.

Case #	FIR+MIR	MIR
1.2	0.1	0.1
2.2	0.03	0.05

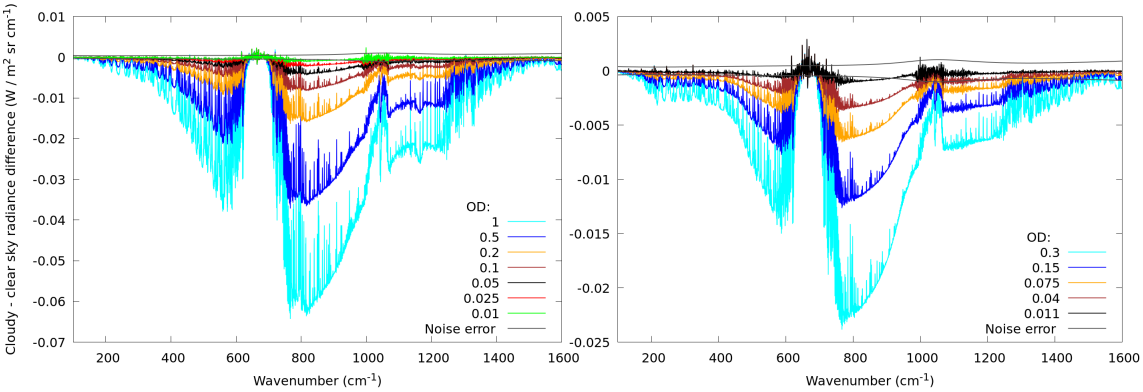

Figure 15. Difference between the TOA radiance in cloudy case for various optical depths of the clouds and the clear sky case of case 1.2 (left panel) and case 2.2 (right panel), compared with the measurement error

for these tests they were set to the true values to avoid that a different error in temperature and water vapour had a different impact in the retrievals performed in the two different spectral regions. The results for the two considered cases are reported in Table 11.

For case 1.2 the minimal optical depth was 0.1 for both MIR and FIR+MIR, while for case 2.2 the minimal optical depth was 0.05 when only MIR measurements are used and 0.03 when both FIR and MIR bands are combined. The addition of the FIR band reduces the retrieval error and enhances the accuracy of the retrieval.

Figure 15 reports the differences between the cloudy spectra relative to various optical depths and the clear-sky spectrum in both cases, compared with the random measurement error. Clouds are detectable and cloud parameters retrievable until the contribution of the cloud to the spectrum is larger than the noise. In real life, where the knowledge of the atmospheric profiles is affected by an error and in presence of other systematic errors, the retrieval of the cloudy quantities may be more difficult, but the information provided by this test represents the goal we can aim to reach.

5.3 Tests on heterogeneouos cases

Given the extension of the FSI pixel, the probability that the scene might be heterogeneous is very high. Heterogeneity of the pixel poses different problems in the retrieval of L2 products (either atmospheric profiles, surface temperature and emissivity or cloud information) from TOA radiance. The first issue is that the ISRF is modelled assuming a homogeneous FoV. If the FSI FoV is strongly heterogeneous, the ISRF may not well represent the instrumental response, thus introducing an error in the retrieval. In the case in which some predominant homogeneous characteristics can be identified in the heterogeneous scene, it is useful to quantify the error in the retrieval of the predominant homogeneous contribution due to the contamination of the scene with clouds or heterogeneities in the surface. On the contrary, if the scene is so heterogeneous that predominant homogeneous characteristics cannot be identified, the measured spectrum has a value in itself, but the information extracted by the L2 analysis is just a combination of contributions coming from the different parts of the sounded atmosphere and surface. The different types of heterogeneities that can occur in the pixel is manifold and the impact of heterogeneities in different scenarios can be very different. A large effort ~~was made in the development of the SGM to handle~~ in the SGM was devoted to the handling of heterogeneous scenes, primarily to study the impact of these heterogeneities on the spectrum and then on the retrieved quantities. In the standard approach used by the L2M module the pixel is assumed to be homogeneous, and the retrieval is performed in either clear sky or cloudy sky condition on the basis of the CIC estimates. Thus, at the moment, we regard any heterogeneity of the FSI FoV as a contamination of either a clear or a cloudy homogeneous scene.

5.3.1 Heterogeneities in the FSI FoV: convolution with ISRF

The objective of this test is to check whether the ISRF, which is modelled assuming a homogeneous FSI FoV, allows a good representation of the ~~radiance resulting from the OSS~~ FSI spectrum also in presence of heterogeneities in the FSI FoV. The ~~FSI~~ OSS is able to accurately reconstruct the radiance seen by the instrument taking care of the different beams coming from different parts of the FoV. L2M simulates the spectrum observed by the instrument by convolving the high resolution spectrum generated by the forward model with the ISRF computed assuming a homogeneous FoV, and hence the deformations in the ISRF introduced by the heterogeneities are neglected. This may have a large impact on the quality of the retrieval, since the information on the profiles at the different altitudes comes from the knowledge of the line shapes of the spectral lines. The magnitude of the impact depends on the heterogeneities which are considered. Given the cylindrical symmetry of the FSI, heterogeneities in the FoV that are expected to mostly affect the ISRF are the ones that have a strong dependence on the radius.

To this purpose, we performed the following test. In the homogeneous case 1.1 we considered the spectrum calculated by the OSS and the one obtained by convolving the high resolution spectrum generated by SGM with the ISRF. We compared the difference between these two spectra with the error noise. ~~We~~ We then repeated the same comparison, this time using a cirrus covering only a part of the pixel in the center of the FoV. ~~In this case we used the SGM high resolution averaged spectrum, convolved with the ISRF and compared with the OSS spectrum.~~

Figures 16 and 17, show, respectively for the homogeneous case and the heterogeneous one, the FSI FoV and the difference between the ~~radiance outgoing the FSI~~output radiance of the FSI, as calculated by the OSS, with the radiance ~~computed~~

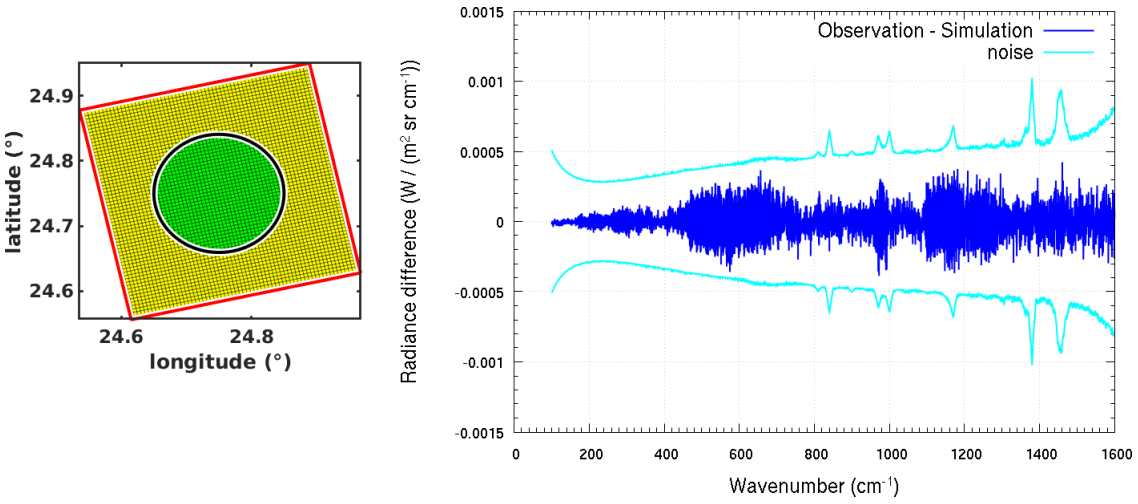

Figure 16. Left panel: FORUM FoV: FEI FoV (yellow), FSI FoV: clear (green). Right panel: difference between the output radiance of the FSI and the ~~simulation of the OSS~~ high resolution SGM radiance convolved by L2M ~~by convolution of the high resolution~~ with the ~~ILS~~ISRF, compared with measurement noise, in the homogeneous case.

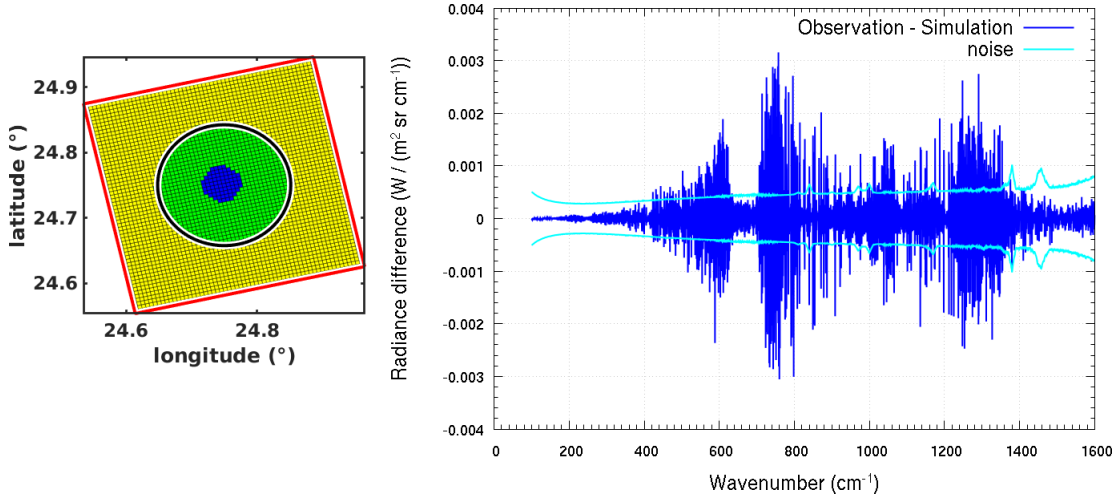

Figure 17. Left panel: FORUM FoV: FEI FoV (yellow), FSI FoV: clear (green) and cloudy (blue). Right panel: difference between the output radiance of the FSI and the ~~simulation of the OSS~~ high resolution SGM radiance convolved by L2M ~~by convolution of the high resolution~~ with the ~~ILS~~ISRF, compared with measurement noise, in the heterogeneous case.

obtained by convolving the high resolution spectrum computed by ~~the forward model~~ SGM with the ISRF. This difference is plotted as a function of the wave number, together with the measurement noise.

In case of a homogeneous scene the convolution with the ISRF is a good representation of the instrumental response. On the contrary, when strong heterogeneities are present, the convolution with the ISRF introduces an error larger than the measurement noise. In principle, the error coming from the representation of the ISRF cannot be neglected in presence of large discontinuities as the ones we have considered. However, the heterogeneity of the scene poses anyway problems to the retrieval module, which considers the scene to be homogeneous. Also, the meaning of the retrieved quantities is uncertain since the measured spectrum represents a kind of average of the different scene characteristics.

In the future, the L2M approach can be developed to use information coming from FEI image and chi-square to identify and define dedicated strategies for heterogeneouos scenes.

5.3.2 Cloud contamination of clear sky FoV

This test aims at estimating the impact that an unidentified cloud contamination of the FSI FoV has on the retrieval, performed with the assumption of clear sky conditions, of temperature and water vapor profiles, and of the surface temperature and frequency dependent emissivity. The test is performed by simulating with the SGM a clear sky scene, which is progressively contaminated by a cloud entering in the FSI FoV. This is the most simple and idealized case, with only two distinct FoV fractions internally homogeneous, that is investigated as a reference case. In real conditions, larger heterogeneities can be observed within the FoV. For this specific test, the study case 1.1/1.2 (tropical profile on desert surface) is used~~. The parameters of the cloud which contaminates the clear-sky scene correspond to an optically thin cirrus cloud : top = 12 ; thickness = 2 ; OD = 1; Reff = 10~~ , with the contaminating cirrus cloud as in test 1.2. The surface properties, as well as the atmosphere, are assumed homogeneous for the entire scene. The FoV fraction occupied by the cloudy sector is increased at steps of 2.5% from 0 to 10%, then at steps of about 7% up to 25% cloud coverage fractions.

Figure 18 reports the simulated spectra and residuals of the fit in the various cases. We note that by increasing the cloud contamination, the residuals depart from purely random ones since the retrieval is not able to compensate for the cloud contamination by changing the retrieved quantities.

The retrieval is performed for each simulation by assuming clear sky conditions, and the retrieved quantities are compared with the values used by the SGM to simulate the part of the scene in clear-sky. These are indicated as the true values. Figure 19 shows the differences between ~~true and retrieved~~ retrieved and true values for the temperature profiles (left panel) and the water vapor profiles (right panel), compared with the corresponding retrieval error for different cloud contamination percentages. In general, increasing the cloud contamination increases the difference of the retrieved temperature profile with respect to the true expected values. In the worst case, at about 700 hPa, the differences increase from within the error for the completely clear sky case (red line) up to about six times larger than the error for the case 97.5% clear — 2.5% cloudy (black line). Similar results, but with a reduced magnitude, are observed for the water vapor profile retrieval. The surface skin temperature retrieval is also affected by the cloud contamination. Figure 20 shows the difference between the true and the retrieved values of the surface emissivity as a function of the clear sky FoV fraction (red line) and the corresponding χ^2 values (green line).

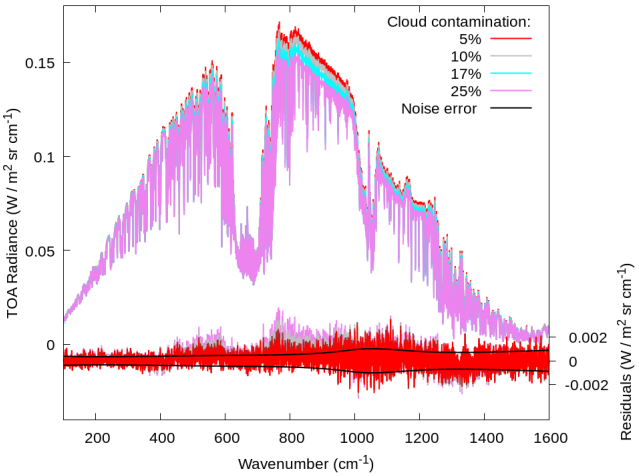

Figure 18. ~~Differences between retrieved~~ Simulated radiances and ~~true profiles for temperature (left panel) and water vapour (right panel) for different percentage~~ residuals of ~~cloud contamination~~ the fit in the ~~FSI FoV, compared with the retrieval noise.~~ various cases

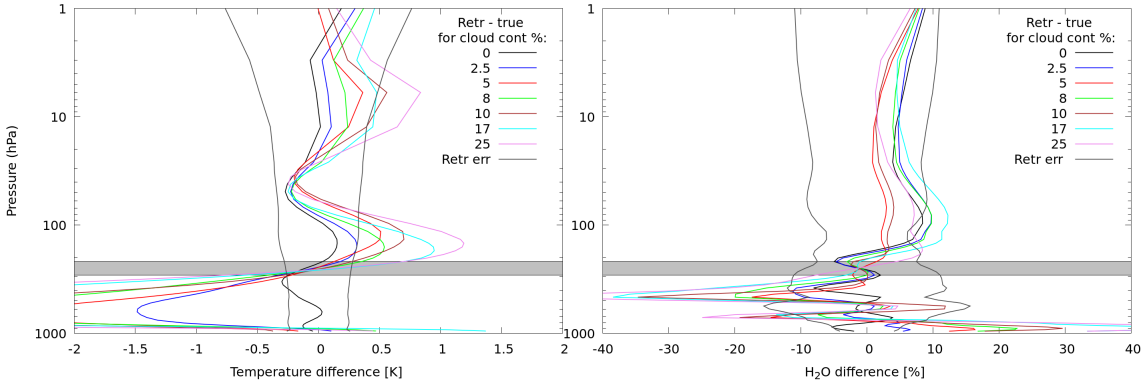

Figure 19. Differences between retrieved and true profiles for temperature (left panel) and water vapour (right panel) for different percentage of cloud contamination in the FSI FoV, compared with the retrieval noise. The cloud pressure range is reported in grey.

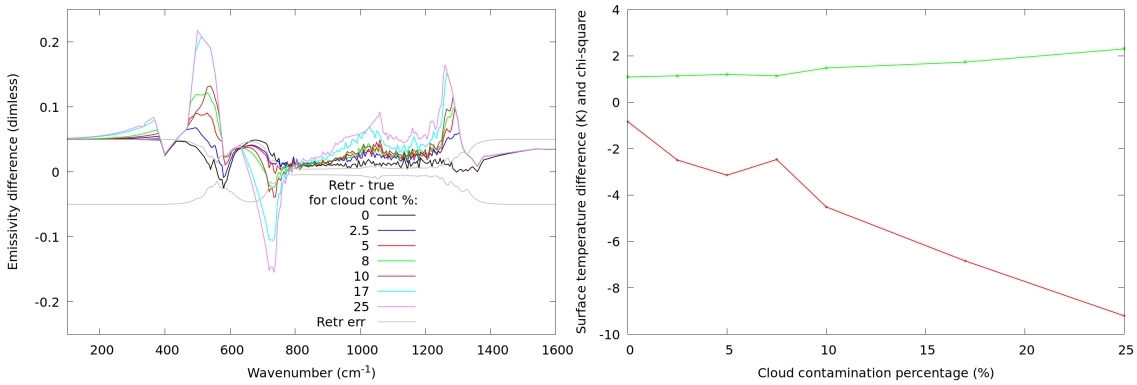

Figure 20. ~~Right plot~~Left panel: Difference between retrieved and true values of surface emissivity for various percentage of cloud contamination in the FSI FoV, compared with the retrieval noise. ~~Left plot~~Right panel: Differences between ~~true and~~ retrieved and true value of surface temperature for various percentage of cloud contamination in the FSI FoV, compared with the retrieval noise. ~~Also the~~ The final chi-square values are also reported~~for all cases~~.

The differences in the retrieved temperature rapidly increase up to 3 K for a 5% cloud contamination in the tested scenario. As described in Subsection 5.1.2 a negative bias in the surface temperature is compensated by a positive bias in the surface emissivity. Since the considered cloud is an optically thin cirrus cloud (OD=1), we expect that for thicker clouds, such as in case of cumuli or cumulonimbi, the effects on the observed radiance and hence on the retrieved skin temperature are larger even for lower fractional areas. For the tested scenario, the quality of the retrieval is compliant with the E2ES requirements for a cloud contamination smaller than 10%. Nevertheless, the CIC algorithm applied to the simulations identified the scene as cloudy as soon as the cloud fraction grew above 8%. This means that the automatic inversion procedure would switch to the cloudy case and would not try to retrieve the surface properties in the worst scenarios, where the errors are too large, preserving the performance of the L2M_I.

5.3.3 Clear sky, heterogeneities in the surface

This test aims ~~to evaluate~~ at evaluating the impact of the heterogeneity of the surface on the retrieval of temperature and water vapour profiles. It is performed for a polar scene, since the largest information on the surface is obtained mainly in the polar regions where the atmosphere is drier and hence more transparent. The scene at the geolocation corresponding to case 5.1 (polar case) is simulated assuming that the surface has a part covered with fine snow and a part covered with sea. The surface temperature used to generate observations changes accordingly, being 273.27 ~~K~~ K on water and ~~258.055 K~~ 254.45 K on snow. Temperature and water vapour profiles are assumed homogeneous in ~~all~~ the sounded atmosphere over the pixel. We used 1 for emissivity a-priori and 253.423 K for surface temperature, a perturbation of the snow value. Results are shown for scenes covered with different percentages of water and snow.

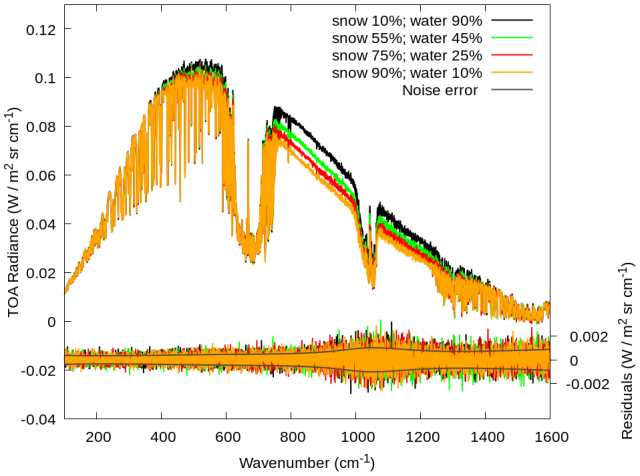

Figure 21. ~~Retrieved profiles~~ Simulated radiances and residuals of the fit for different ~~types~~ percentages of ~~soil heterogeneity for emissivity, and true profiles for homogeneous snow (cyan) and~~ water~~(blue) soils~~/snow FoV coverage indicated in the legend

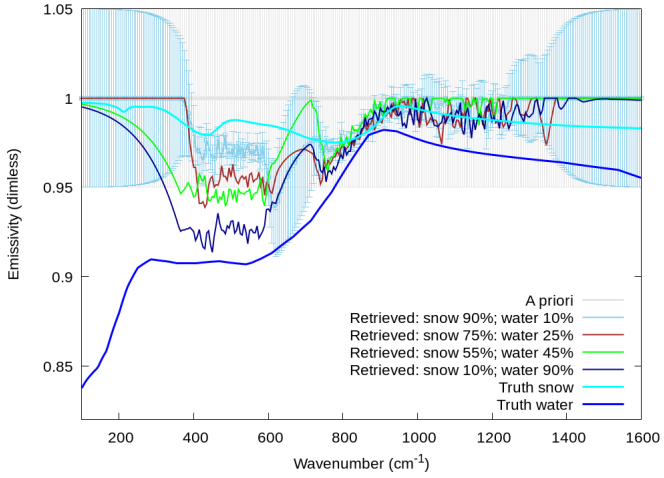

Figure 22. Surface emissivity retrieved profiles for different types of soil heterogeneity, and true profiles for homogeneous snow (cyan) and water (blue) soils. The used a priori profile and relative error is shown in grey. For readibility reason the retrieval error is shown only for one case (snow 90%-water 10%), but the other cases are characterised by similar errors.

Figure 21 reports the simulated spectra and residuals of the fit for different percentages of water/snow FoV coverage (snow 10%, 55%, 75%, 90%). The residuals in all cases are compatible with the measurement noise and show no bias.

Figure 22 reports the retrieved emissivity in the various cases, while the retrieved surface temperature is reported in Table 12.

Table 12. Retrieved surface temperature for different percentages of water/snow FoV coverage.

~~Case~~snow% in FSI FoV	~~Percentage of pixel surfacecovered with snow~~ water% in FSI FoV	~~Percentage of pixel surface covered with water~~ Weighted tskin	Retrieved ~~surfa~~
~~1~~ 10	90	~~270.3~~270.8	
~~3~~ 55	~~25~~ 45	~~75~~ 262.9	
~~2~~ 75	~~55~~ 25	~~45~~ 259.1	
~~4~~ 10	90	~~10~~ 256.9	

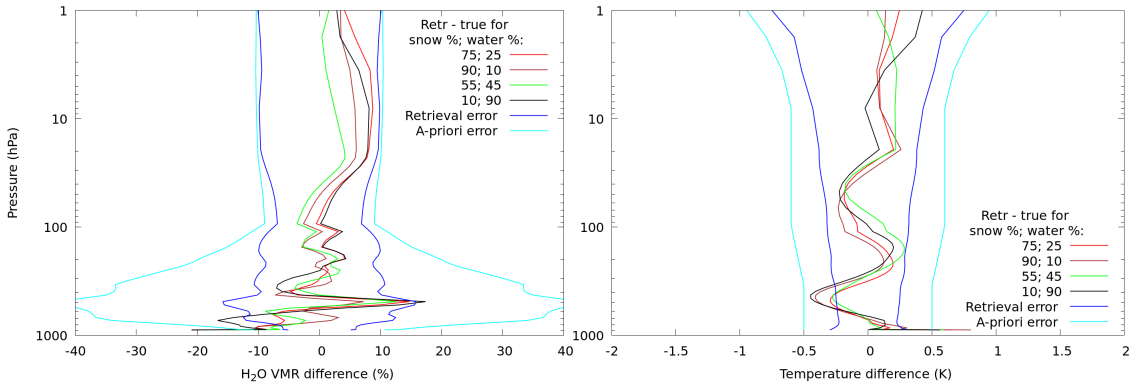

Figure 23. Differences between retrieved ~~profiles~~ and ~~the truth~~ true profiles for different types of soil heterogeneity for temperature (left plot) and water vapour (right plot). Retrieval and a-priori errors are also shown.

In all cases we find that retrieval of surface emissivity, as well as surface temperature, ~~change for the different cases, with retrieved values in~~ adapts in an almost linear way to handle the different percentage of snow/water pixel coverage, in particular in the spectral region between 400 and 600 cm^{-1}, where water and snow emissivity mostly differ, ~~being always~~ the retrieved emissivity is closer to the water ~~surface emissivity despite the percentage of pixel coverage of the water surface . No bias is introduced by the heterogeneous pixel in the retrieval of~~ or the snow surface emissivity according to the predominance percentage of the surface type in the pixel coverage. Differences between retrieved products and the weighted mean of the emissivities characterizing the different pixels of the FoV have to be attributed to the negative correlation between surface temperature and emissivity. On the contrary, the retrieved water and temperature profiles are little affected by the surface heterogeneities, since the differences between the retrieved value and the true one are always within the retrieval error (see Figure 23).

Table 13. Scene definition for heterogeneous MODIS cases.

Case #	Geolocation	Time	Description
M.1	52.70°N / 1.85°W	7 Feb 2018, 13:30	Clear sky over land
M.2	53.50°N / 2.00°W	7 Feb 2018, 13:30	High cirrus clouds over land
M.3	51.38°N / 4.15°W	7 Feb 2018, 13:30	High cirrus clouds over sea

5.3.4 ~~Realistic tests~~ Tests based on MODIS ~~data~~L2 products

All the previously investigated scenarios rely on idealized conditions, where the surface and, eventually, the cloud layer can only have homogeneous properties within the FSI FoV or a simple binomial characterization. This simplified scene description is convenient to evaluate study case scenarios and to guarantee a good computational speed of the E2ES chain. Unfortunately, the real world is far from being ideal and almost homogeneous conditions are more likely the exception rather than the rule. Surface, atmosphere, and cloud properties can significantly vary on spatial scales of the order of few kilometers or less, and their effects combine into a single 15 km diameter FoV FSI observation.

This last test aims at evaluating the E2ES performance in case a realistic, largely heterogeneous scene is ingested by the L2M module. Three complex case studies are generated with the SGM: a clear sky case (M.1) over land, where the scene heterogeneity depends on the surface properties (temperature and emissivity) and on the atmospheric profiles (temperature and water vapor concentration); two cloudy sky scenes over land (M.2) and sea (M.3), where the clouds inhomogeneities sum up with those of surface and atmosphere. Close locations in southern England are selected, whose geolocation and time are reported in Table 13.

The ~~necessary parameters~~ surface, atmospheric and cloud parameters used to build the scene are derived from the following databases~~, homogenized and remapped into the FEI grid~~:

- Surface emissivity: the Global Land Cover Map (GlobCover 2009, http://due.esrin.esa.int/page_globcover.php) is an ESA's composite product based on MERIS (Medium Resolution Imaging Spectrometer Instrument) data collected at 300 m spatial resolution. The GlobCover map provides 22 land cover classes, defined with the United Nations land cover classification system, that are associated to the 11 surface types from ~~Huang et al. (2016)~~ Huang et al. (2016) used in the SGM surface definition;

- Atmosphere: the MODIS Atmospheric Profile product (07_L2, https://modis-images.gsfc.nasa.gov/products.html) defines the temperature and water vapor profiles, and the surface height at 5 km resolution;

- ~~Clouds~~Cloud properties and surface temperature: the MODIS Cloud Product (06_L2) are used to define the cloud parameters (particles phase and effective radius, cloud top height and optical thickness) and the surface temperature, with spatial resolution of 1 km.

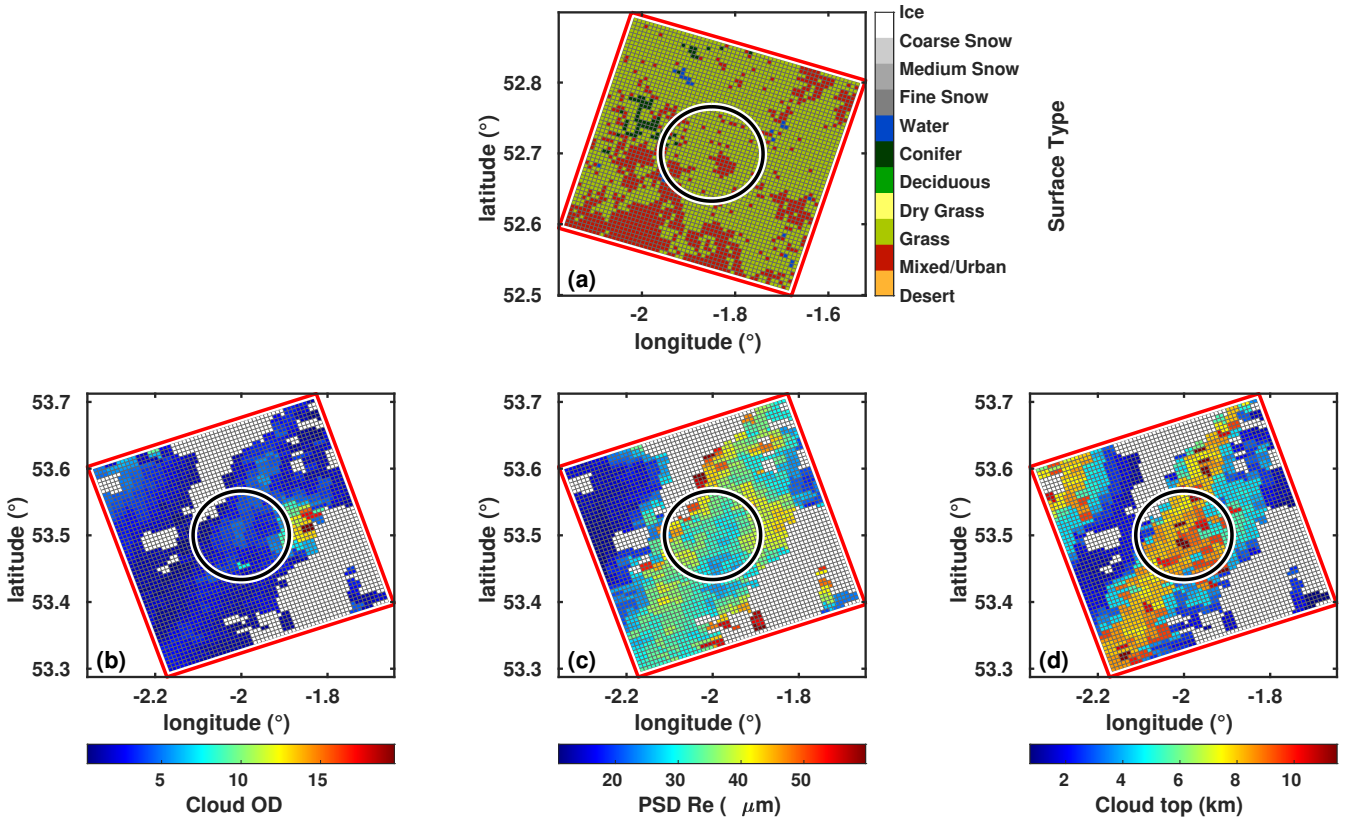

Figure 24. Top panel: Surface type for the study case M.1, derived from GlobCover database and remapped on the FEI grid. The FSI FoV is marked with the black ring. Bottom panels: Cloud optical depth at 900 cm^{-1} (left), PSD effective radius (center), and cloud top height (right) for the study case M.2, derived from MODIS L2 data and remapped on the FEI grid. White areas indicate clear sky.

~~Note that the SGM is not designed to build such complex scenes for the standard~~ The above products are characterized by different grids and spatial resolutions; thus, they are remapped into the FEI grid. Once the cloud, atmospheric and surface information are available at the same grid, a dedicated subroutine, mimicking the SGM, is applied to compute the spectral radiance for each pixel. Due to the complexity of the process the subroutine is kept external to the E2ES ~~configuration. These scenarios are built with a dedicated subroutine and~~ chain. Nevertheless, following the above procedure, multiple scenarios can be built from satellite products for complex atmospheric conditions. The radiances are stored in the E2ES ~~chain for the testing activities only~~as ancillary data and used for testing the FORUM E2ES performances on realistic conditions.

Figure 24 shows ~~few~~ examples of the surface and cloud parameters remapped into the FEI grids. The scene observed in the M.1 clear sky case (top panel) has irregularly sparse urban areas (brown) surrounded by different kinds of vegetation (light and dark green) and few wet areas (blue, probably lakes or ponds), creating a much more complex scenario than an ideal homogeneous case. Similarly, clear sky areas alternate to high and low level clouds, with unevenly distributed optical and

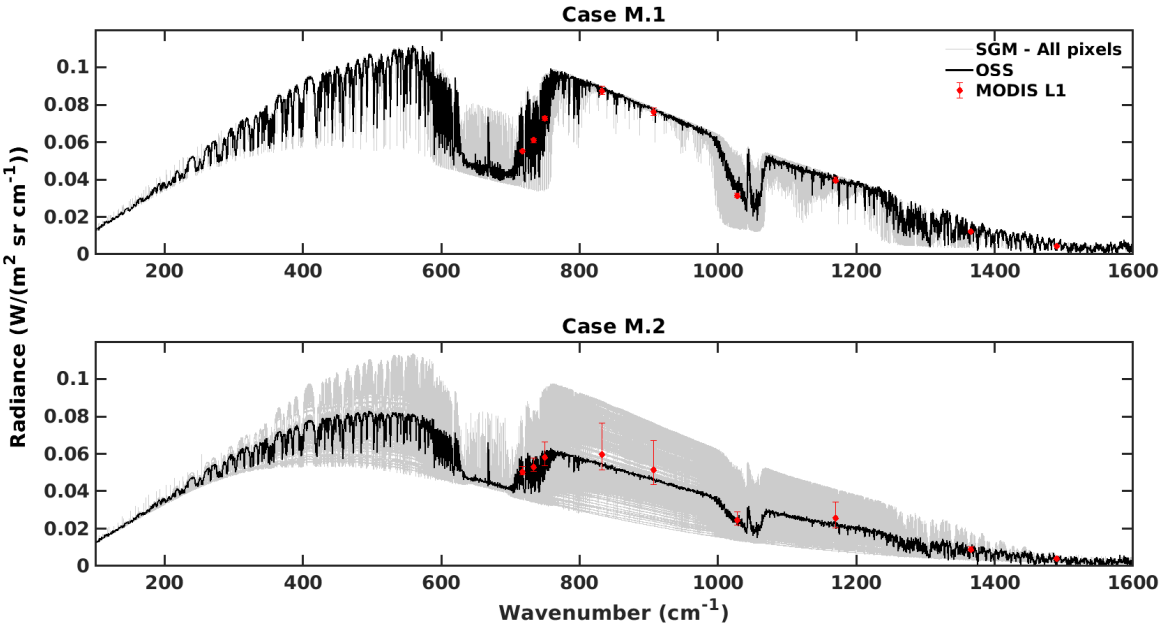

Figure 25. Spectral radiances computed by using the dedicated subroutine mimicking the SGM (grey lines) for each FEI pixel within the FSI field of view are plotted with radiances obtained from the FSI-OSS (black lines) for the cases M.1 (top panel) and M.2 (bottom panel). The MODIS radiance at specific bands are also reported in red dots. The vertical red bars indicate the MODIS radiance variability within FSI FoV.

microphysical parameters, in the cloudy case M.2 (bottom panels). ~~Thus, multiple~~ Multiple spectral radiances are computed by the SGM for all the FEI grid points within the FSI FoV (the black ~~ring in the Figures~~circle in the panels of Figure 24), according to the different properties of the scene. ~~Then, the radiances are linearly combined~~ Within the E2ES, the pre-computed radiances are ingested by the FSI-OSS module to produce a single spectral radiance~~to feed the~~ . In figure 25 the spectral radiances computed for each FEI pixel inside of the FSI FoV (by using the dedicated subroutine mimicking the SGM) are plotted together with the FSI-OSS ~~module.~~ output radiance for the cases M.1 and M.2. The figure also reports radiance measurements in multiple MODIS channels (red dots) with their variability within the FSI FoV. Note that the FSI-OSS spectral radiance based on MODIS products and the mean MODIS radiance at specific bands are consistent, but a perfect match is not expected due to the non-linearity between L2 products and the radiance.

Finally, the L2M is used to retrieve the characterizing parameters of the complex scenes, in particular: temperature and water vapour profiles, and surface skin temperature and emissivity for the case M.1, correctly classified by CIC as a clear sky scene; cloud properties for the cases M.2 and M.3, classified by CIC as ~~cloudy scenes.~~a cloudy scene."

In the analysed realistic cases, it is not possible to define a single *truth* to be compared with the retrieval results. The average parameters within the FSI FoV do not properly describe the scene as a whole. To evaluate the L2M_I performance, the

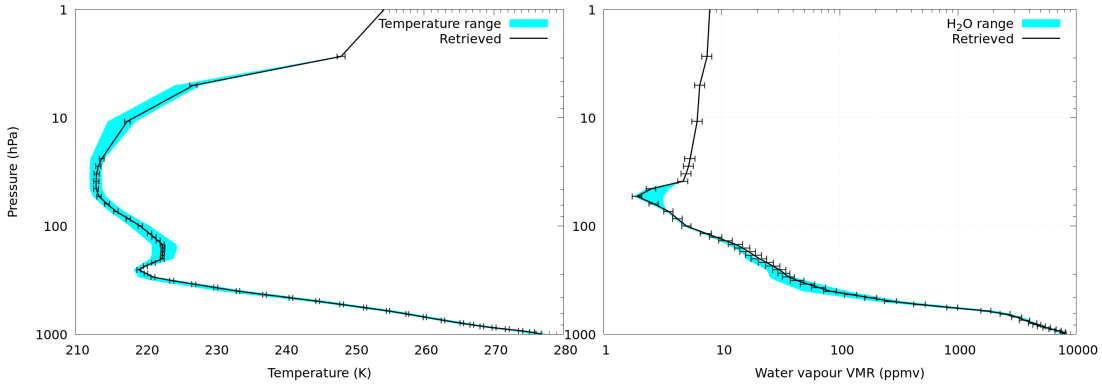

Figure 26. Comparison between the retrieved ~~parameters~~ profiles and the ~~input~~ reference ~~ones~~ profiles for the clear sky case M.1. Top left, temperature profiles ~~for~~ range in the FoV ~~pixels~~ and retrieved profile with retrieval error. Top right, water vapor profiles range for the FoV ~~pixels~~ and retrieved profile with retrieval error. Bottom, emissivity profiles with percentage in the FoV pixels, a priori, weighted emissivity average and retrieved profile with retrieval error.

assessment test verifies that the retrieved scalar quantities lie within one standard deviation from the average value, and that spectral quantities and profiles are consistent, within the error bars, with the bulk of the input values.

Figure ~~??~~ 26 shows the retrieval results (black curves) of the clear sky case M1. ~~Temperature~~ Retrieved temperature and water vapor profiles ~~(upper panels)~~ are compared with ~~all the~~ the range of the reference profiles that are considered for the SGM simulation within the FSI FoV, derived from the MODIS L2 data. The retrieved profiles are consistent with the input profiles along the entire vertical extension of the model. ~~The bottom panel shows~~

In figure 27 the emissivity retrieval is reported. As already shown in Section 5.1.2, the sensitivity to surface emissivity at mid-latitudes is limited to the spectral range 700–1300 cm^{-1}, because of the large absorption of water vapor in the FIR. We show the emissivity profiles used by the SGM along with the percentage of FoV pixels. The retrieved emissivity in the atmospheric window is very close to the weighted average of the input profiles, suggesting the capabilities of the inversion procedure in a complex scenario. Finally, the model surface skin temperature of 275.96 ± 0.05 K is well reconstructed by the retrieved value 276.12 ± 0.39.

Table 14 shows the retrieval results for the two cloudy sky cases, M.2 and M.3 respectively. The retrieved cloud parameters (optical depth, PSD effective radius, and cloud top height) are scalar values, therefore, they are compared with the range of the same parameters for all the FSI FoV subpixels. As in the previous case, despite the heterogeneity of the observed scene, the L2M retrieves values that are in the range of the observed scene. There is a slight tendency to overestimate the particle radius, but for large particles there is no sensitivity in the measurements. These tests further confirm the good performance of the E2ES as a tool for the analysis of ideal and realistic study cases.

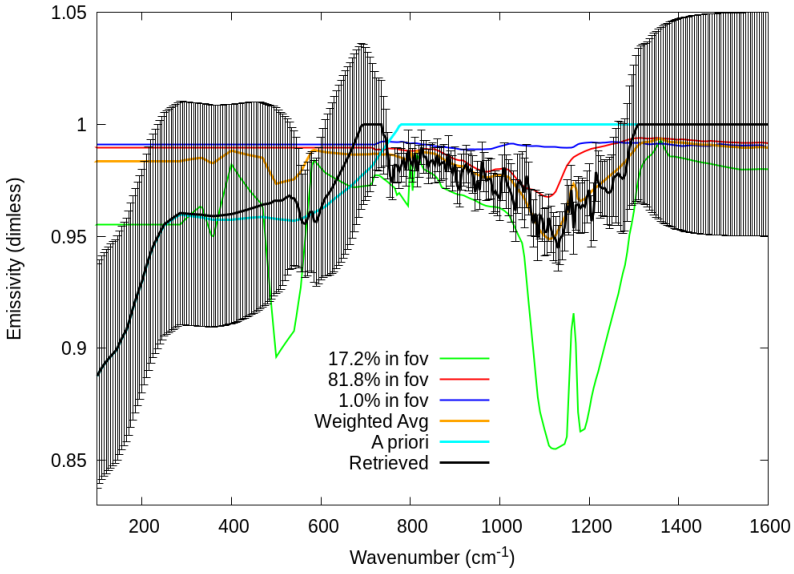

Figure 27. Emissivity profiles with percentage in the FoV pixels, a priori, weighted emissivity average and retrieved profile with retrieval error.

Table 14. Cloud parameter results for cloudy MODIS cases M.2 and M.3.

Property	Reference	Retrieved
Case M.2		
Cloud Top Height	2.—11.5	9.00 ± 0.07
Optical Depth	0.51—9.66	2.04 ± 0.04
Particle Size	24.3—50.7	67.11 ± 0.08
Case M.3		
Cloud Top Height	7.0—11.5	10.04 ± 0.03
Optical Depth	0.74—3.98	1.44 ± 0.06
Particle Size	10.9—23.7	31.95 ± 0.05

6 Running time

The E2ES was not designed with computing time optimization in mind. For this task an adaptation to FORUM of fast forward models such as σ-IASI (Amato et al., 2002) would be more adequate. However, in order to run all the tests, some effort has been devoted to code speedup. Almost all the computing time of the E2ES is spent in two tasks, the remaining components affect only marginally the results.

1. The forward model calculation, i.e. running LBLRTM in clear sky cases and fDISORT in cloudy sky cases. This task is performed by the SGM as many times as the number of not homogeneous pixels in the scene, and by L2M_I as needed by the retrieval sequence.

2. The ISRF convolution. This task is only performed by L2M_I. Given the frequency-dependent characteristic of the ISRF, the task needs to be performed in the radiance domain and the FFT cannot be applied.

Of course the computing time heavily depends on the machine used and on the compiler. The figures presented are referred to a Intel(R) Xeon(R) CPU E5-1650 v2 @ 3.50GHz machine with six physical cores, and to the Intel ifort compiler.

The scene preparation, consisting in reading the user input parameters and setting the input files for the forward computations, is very fast and typically lasts about 5 seconds.

The typical running speed for the LBLRTM, with an optimized spectroscopic database, is 35–40 seconds, with no major differences between scenes. The running time of fDISORT is the bottleneck of the cloudy retrieval, and it is heavily dependent on the cloud composition. A larger number of layers of the cloud, larger particles and larger OD tend to increase the computation time of the multiple scattering effect. The running time of the fDISORT, if executed serially, varies from 20 minutes (cirrus cloud of case 1.2) to 30 hours (thick opaque cloud of case 6.2). The fDISORT is itself between 1.2 (for liquid clouds) and 3.7 (for cirrus clouds) times faster than the original DISORT (Sgheri and Castelli, 2018). Applying optimizations of Section 5.2.2, the thick cloud fDISORT is ten times faster.

As for the convolution, a single operation takes about 20 seconds, but the tasks needs to be repeated at each iteration for each point of the vertical profiles of temperature and water vapour, plus two times for skin temperature and emissivity. For clear sky cases in the standard settings we need 106 convolutions at each iteration.

The running time of the SGM in a homogeneous situation is approximately equal to that of the LBLRTM for the clear sky cases, and that of the fLBLDIS for the cloudy sky cases. It is evident that in the case of the MODIS scenes, where each sub-pixel of the FSI FoV is treated separately, the SGM radiances had to be pre-computed, because the calculations last several days, even with parallelization of the tasks.

The L2M_CIC module only takes less than one minute to perform the land mask, the cloud identification and classification, the characterization of the level of inhomogeneities in the FSI pixel, and the preparation of the first guess inputs for the cloud retrieval.

For the L2M_I module we take advantage of the multi-core feature of the machine. The fDISORT is computed in parallel over different wave number intervals running multiple copies of the external binary, with results close to the theoretical maximum

speedup. The convolution is computed using the multi-thread support of the OpenMP (OpenMP Architecture Review Board, 2018) libraries. With these settings, the effective running time is still affordable to run tests, even in cloudy sky situations.

For the clear sky cases the running time of each iteration of the L2M_I module is about 20–25 minutes. The full L2M_I clear retrieval, including ancillary tasks such as the additional forward model after the regularization to calculate the chi-square of the regularized solution, takes about 90 minutes for case 1.1 that uses four iterations.

For the cloudy sky cases the running time of each iteration of the L2M_I module varies from the 10–12 minutes of case 1.2 to the 90–120 minutes of case 6.2. In the cloudy cases the longest execution time of the forward model is compensated by the fact that we only retrieve the cloud parameters, using a constant perturbed atmosphere. The pre-processor, which is only enabled for cirrus clouds, takes about 30 minutes. The full L2M_I cloudy retrieval takes about 120 minutes for case 1.2 that uses five iterations, and 440 minutes for case 6.2 (the longest) that uses three iteration, but also needs three Marquardt micro-iterations.

7 Conclusions

The findings of the FORUM E2ES project are presented. In the ~~E2E~~ E2ES the geometry of the orbit, the atmosphere and the FSI and FEI instruments are fully modeled with realistic configurations and retrieval is performed assuming either full clear sky or ~~cloudy-sky~~ cloudy sky scenes.

We first successfully validate the performances of the ~~E2E~~ E2ES chain with correlative codes, a necessary step to ensure that there are no flaws. Then, we select some homogeneous test cases, both in clear and in cloudy sky, chosen to represent all different atmospheric conditions, soil characteristics and cloud types. In all cases, the retrieved quantities satisfy FORUM requirements. In cloudy sky, we also show that the optical depth threshold for a cirrus to be detected varies between 0.03 and 0.1, with generally better sensitivity if the FIR is included. The threshold depends on the different characteristics of the surface and the atmosphere.

The influence on the retrieval of inhomogeneities in the field of view is also investigated. The convolution of the high resolution spectrum with the ISRF function (computed assuming a model homogeneous FoV) well represents the instrumental effects for a homogeneous FoV, with the error being below the NESR threshold. This is not the case when a strong inhomogeneity is considered.

Heterogeneous soil in the FoV does not impact the retrieval of atmospheric profiles, with the retrieved surface temperature and emissivity approaching the weighted averages of the surface properties.

Even ~~a~~ small contamination of a cloud in the FoV induces errors in the retrieved atmospheric and surface quantities. The error increases with the increase of the percentage of the FoV affected by the contamination and of the optical depth of the cloud. However, it is important to underline that, by exploiting the information content of the FIR channels, the CIC algorithm is highly sensitive to the presence of a cloud in the FSI FoV, even with a low percentage of cloud contamination. Thus, in most cases, the cloud identification is performed and the performances of the L2M_I are preserved. Note that CIC is the first algorithm which exploits the far infrared spectral interval for cloud identification and classification from satellite observations,

including the determination of cloud phase. In particular, it is demonstrated that the combined use of FIR and MIR spectral radiances enhances the cloud detection performances achievable by using the MIR part of the spectrum only.

Finally we perform the retrieval on some realistic, heterogeneous scenes, which, however, present a predominance of either clear sky or cloudy sky. We show that the retrieval converges to values that are included in the range of variability of the quantities used to model the radiances.

~~The E2E chain has been used to show how the instrument characteristics and scene conditionsimpact on the spectrum measured by the instrument, and the consequences on the retrieval process. Critical issues have been highlighted.~~

~~These issues should be addressed both by developing a more sophisticated retrieval approach, and by exploring the best way to~~ Some critical problems have been highlighted. In particular, we believe the following main issues should be investigated, also considering the best way to use the IASI-NG sinergy.

- Emissivity retrieval. The retrieval method and grid should be optimized, as it is clear from the tests of this paper. Some work is being done (Ben-Yami et al., 2021) in clear sky. The preliminary tests in cloudy sky conditions, with an evolution of the code that retrieves simultaneously the atmospheric and cloud parameters, show that this issue will be even more important, given the reduced sensitivity to the atmospheric surface due to the cirrus cloud.
- Atmospheric retrieval in presence of thick clouds. In this case there is no sensitivity to atmospheric parameters below the cloud top. A clear sky retrieval can be attempted with the cloud top representing the bottom limit for the radiative transfer, similarly to Feng et al. (2021).
- Heterogeneous FoV. In this case we might employ the FEI results to determine a homogeneity map for the various parts of the FSI FoV. This can be seen as an a-priori to attempt a composite (partly clear, partly cloud) retrieval.

Author contributions. All authors contributed to the writing of this paper. **Claudio Belotti** wrote the L2M python wrapper. **Maya Ben-Yami** performed some tests. **Giovanni Bianchini** was responsible for the OSS module, and wrote the FSI code. **Bernardo Carnicero Dominguez** was the FORUM Phase A study manager. **Ugo Cortesi** coordinated the contacts between CNR and DEIMOS. **Samuele Del Bianco** was responsible for the E2ES validation, and performed the tests in clear sky. **Gianluca Di Natale** performed the validation tests in cloudy sky. **Tomás Guardabrazo** was the E2ES project manager, contributed the geometry module and wrote the FEI and PAM modules. **Dulce Lajas** was the E2ES FORUM ESA's Technical Responsible during the FORUM Phase A and Phase B1. **Tiziano Maestri** was responsible for the SGM module. **Tiziano Maestri**, **William Cossich** and **Davide Magurno** wrote the SGM and L2M_CIC code. **Hilke Oetjen** is the FORUM Mission Scientist. **Piera Raspollini** was responsible for the assessment campaign, and performed most of the tests of this paper. **Cristina Sgattoni** performed some tests. **Luca Sgheri** was responsible for the L2M module, wrote the L2M inversion code and coordinated the writing of this paper.

Competing interests. No competing interests are present

Acknowledgements. We would like to thank all the FORUM research group, a large and active community. Only by working together the FORUM project grew from an instrument concept to an operative mission.

References

Amato, U., Masiello, G., Serio, C., and Viggiano, M.: The σ-IASI code for the calculation of infrared atmospheric radiance and its derivatives, Environmental Modelling & Software, 17, 651–667, https://doi.org/10.1016/s1364-8152(02)00027-0, 2002.

Ben-Yami, M., Oetjen, H., Brindley, H., Cossich, W., Lajas, D., Maestri, T., Magurno, D., Raspollini, P., Sgheri, L., and Warwick, L.: Emissivity Retrievals with FORUM's End-to-end Simulator: Challenges and Recommendations, Atmospheric Measurement Techniques Discussions, 2021, 1–36, https://doi.org/10.5194/amt-2021-232, 2021.

Bianchini, G. and Palchetti, L.: Technical Note: REFIR-PAD level 1 data analysis and performance characterization, Atmospheric Chemistry and Physics, 8, 3817–3826, https://doi.org/10.5194/acp-8-3817-2008, 2008.

Bianchini, G., Carli, B., Cortesi, U., Del Bianco, S., Gai, M., and Palchetti, L.: Test of far-infrared atmospheric spectroscopy using wide-band balloon-borne measurements of the upwelling radiance, Journal of Quantitative Spectroscopy and Radiative Transfer, 109, 1030–1042, https://doi.org/https://doi.org/10.1016/j.jqsrt.2007.11.010, 2008.

Bianchini, G., Palchetti, L., and Carli, B.: Vectorial combination of signals in Fourier transform spectroscopy, Infrared Physics & Technology, 52, 19–21, https://doi.org/https://doi.org/10.1016/j.infrared.2008.09.004, 2009.

Bianchini, G., Castagnoli, F., Di Natale, G., and Palchetti, L.: A Fourier transform spectroradiometer for ground-based remote sensing of the atmospheric downwelling long-wave radiance, Atmospheric Measurement Techniques, 12, 619–635, https://doi.org/10.5194/amt-12-619-2019, 2019.

Bozzo, A., Maestri, T., Rizzi, R., and Tosi, E.: Parameterization of single scattering properties of mid-latitude cirrus clouds for fast radiative transfer models using particle mixtures, Geophysical Research Letters, 35, https://doi.org/10.1029/2008gl034695, 2008.

Brindley, H. E. and Harries, J. E.: The impact of far i.r. absorption on clear sky greenhouse forcing: sensitivity studies at high spectral resolution, Journal of Quantitative Spectroscopy and Radiative Transfer, 60, 151–180, https://doi.org/10.1016/s0022-4073(97)00152-0, 1998.

Carli, B., Bazzini, G., Castelli, E., Cecchi-Pestellini, C., Del Bianco, S., Dinelli, B., Gai, M., Magnani, L., Ridolfi, M., and Santurri, L.: MARC: A code for the retrieval of atmospheric parameters from millimeter-wave limb measurements, Journal of Quantitative Spectroscopy and Radiative Transfer, 105, 476–491, https://doi.org/https://doi.org/10.1016/j.jqsrt.2006.11.011, 2007.

Chahine, M. T., Pagano, T. S., Aumann, H. H., Atlas, R., Barnet, C., Blaisdell, J., Chen, L., Divakarla, M., Fetzer, E. J., Goldberg, M., Gautier, C., Granger, S., Hannon, S., Irion, F. W., Kakar, R., Kalnay, E., Lambrigtsen, B. H., Lee, S.-Y., Marshall, J. L., Mcmillan, W. W., Mcmillin, L., Olsen, E. T., Revercomb, H., Rosenkranz, P., Smith, W. L., Staelin, D., Strow, L. L., Susskind, J., Tobin, D., Wolf, W., and Zhou, L.: AIRS, Bulletin of the American Meteorological Society, 87, 911–926, https://doi.org/10.1175/bams-87-7-911, 2006.

Chen, X., Huang, X., and Flanner, M. G.: Sensitivity of modeled far-IR radiation budgets in polar continents to treatments of snow surface and ice cloud radiative properties, Geophysical Research Letters, 41, 6530–6537, https://doi.org/10.1002/2014gl061216, 2014.

Clough, S., Shephard, M., Mlawer, E., Delamere, J., Iacono, M., Cady-Pereira, K., Boukabara, S., and Brown, P.: Atmospheric radiative transfer modeling: a summary of the AER codes, Journal of Quantitative Spectroscopy and Radiative Transfer, 91, 233–244, https://doi.org/https://doi.org/10.1016/j.jqsrt.2004.05.058, 2005.

Clough, S. A. and Iacono, M. J.: Line-by-line calculation of atmospheric fluxes and cooling rates: 2. Application to carbon dioxide, ozone, methane, nitrous oxide and the halocarbons, Journal of Geophysical Research, 100, 16 519, https://doi.org/10.1029/95jd01386, 1995.

Clough, S. A., Iacono, M. J., and Moncet, J.-L.: Line-by-line calculations of atmospheric fluxes and cooling rates: Application to water vapor, Journal of Geophysical Research: Atmospheres, 97, 15 761–15 785, https://doi.org/https://doi.org/10.1029/92JD01419, 1992.

Cortesi, U., Bianco, S. D., Gai, M., Laurenza, L., Ceccherini, S., Carli, B., Barbara, F., and Buchwitz, M.: Sensitivity analysis and application of KLIMA algorithm to GOSAT and OCO validation - KLIMA-IASI, Final Report of Project ESA-ESRIN/Contract n. 21612/08/I-OL, Tech. Rep. IFAC-TSRR, IFAC-CNR, 2014.

Cossich, W., Maestri, T., Magurno, D., Martinazzo, M., Di Natale, G., Palchetti, L., Bianchini, G., and Del Guasta, M.: Ice and mixed-phase cloud statistics on the Antarctic Plateau, Atmospheric Chemistry and Physics, 21, 13 811–13 833, https://doi.org/10.5194/acp-21-13811-2021, 2021.

Di Natale, G., Palchetti, L., Bianchini, G., and Del Guasta, M.: Simultaneous retrieval of water vapour, temperature and cirrus clouds properties from measurements of far infrared spectral radiance over the Antarctic Plateau, Atmospheric Measurement Techniques, 10, 825–837, https://doi.org/10.5194/amt-10-825-2017, 2017.

Di Natale, G., Bianchini, G., Del Guasta, M., Ridolfi, M., Maestri, T., Cossich, W., Magurno, D., and Palchetti, L.: Characterization of the Far Infrared Properties and Radiative Forcing of Antarctic Ice and Water Clouds Exploiting the Spectrometer-LiDAR Synergy, Remote Sensing, 12, 3574, https://doi.org/10.3390/rs12213574, 2020.

Di Natale, G., Palchetti, L., Bianchini, G., and Ridolfi, M.: The two-stream δ-Eddington approximation to simulate the far infrared Earth spectrum for the simultaneous atmospheric and cloud retrieval, Journal of Quantitative Spectroscopy and Radiative Transfer, 246, 106 927, https://doi.org/https://doi.org/10.1016/j.jqsrt.2020.106927, 2020.

Dinelli, B. M., Castelli, E., Carli, B., Del Bianco, S., Gai, M., Santurri, L., Moyna, B. P., Oldfield, M., Siddans, R., Gerber, D., Reburn, W. J., Kerridge, B. J., and Keim, C.: Technical Note: Measurement of the tropical UTLS composition in presence of clouds using millimetre-wave heterodyne spectroscopy, Atmospheric Chemistry and Physics, 9, 1191–1207, https://doi.org/10.5194/acp-9-1191-2009, 2009.

Dinelli, B. M., Labonnote, L., and Bianco, S. D.: Consolidated recommendations for updating the MRD regarding Level 1 data, and definitions, Technical Note 8, FORUMreq project: FORUM - consolidation of requirements and reference scenarios, 2020.

Eremenko, M., Sgheri, L., Ridolfi, M., Cuesta, J., Costantino, L., Sellitto, P., and Dufour, G.: Tropospheric ozone retrieval from thermal infrared nadir satellite measurements: Towards more adaptability of the constraint using a self-adapting regularization, Journal of Quantitative Spectroscopy and Radiative Transfer, 238, 106 577, https://doi.org/https://doi.org/10.1016/j.jqsrt.2019.106577, 2019.

ESA: Earth Explorer 9 Candidate Mission FORUM, Report for Mission Selection ESA-EOPSM-FORM-RP-3549, European Space Agency, Noordwijk, The Netherlands, https://esamultimedia.esa.int/docs/EarthObservation/EE9-FORUM-RfMS-ESA-v1.0-FINAL.pdf, 2019.

ESA: Far-infrared-Outgoing-Radiation Understanding and Monitoring (FORUM) - Mission Requirements Document, Tech. rep., ESA, Earth and Mission Science Division, 2020.

Feldman, D. R., Collins, W. D., Pincus, R., Huang, X., and Chen, X.: Far-infrared surface emissivity and climate, Proceedings of the National Academy of Sciences, 111, 16 297–16 302, https://doi.org/10.1073/pnas.1413640111, 2014.

Feng, J., Huang, Y., and Qu, Z.: A simulation-experiment-based assessment of retrievals of above-cloud temperature and water vapor using a hyperspectral infrared sounder, Atmospheric Measurement Techniques, 14, 5717–5734, https://doi.org/10.5194/amt-14-5717-2021, 2021.

Han, Y., Revercomb, H., Cromp, M., Gu, D., Johnson, D., Mooney, D., Scott, D., Strow, L., Bingham, G., Borg, L., Chen, Y., DeSlover, D., Esplin, M., Hagan, D., Jin, X., Knuteson, R., Motteler, H., Predina, J., Suwinski, L., Taylor, J., Tobin, D., Tremblay, D., Wang, C., Wang, L., Wang, L., and Zavyalov, V.: Suomi NPP CrIS measurements, sensor data record algorithm, calibration and validation activities, and record data quality, Journal of Geophysical Research: Atmospheres, 118, 12,734–12,748, https://doi.org/10.1002/2013jd020344, 2013.

Hansen, J. E.: Multiple Scattering of Polarized Light in Planetary Atmospheres Part II. Sunlight Reflected by Terrestrial Water Clouds, Journal of the Atmospheric Sciences, 28, 1400–1426, https://doi.org/10.1175/1520-0469(1971)028<1400:msopli>2.0.co;2, 1971.

Harries, J., Carli, B., Rizzi, R., Serio, C., Mlynczak, M., Palchetti, L., Maestri, T., Brindley, H., and Masiello, G.: The Far-infrared Earth, Reviews of Geophysics, 46, https://doi.org/https://doi.org/10.1029/2007RG000233, 2008.

Hersbach, H., Bell, B., Berrisford, P., Hirahara, S., Horányi, A., Muñoz-Sabater, J., Nicolas, J., Peubey, C., Radu, R., Schepers, D., Simmons, A., Soci, C., Abdalla, S., Abellan, X., Balsamo, G., Bechtold, P., Biavati, G., Bidlot, J., Bonavita, M., De Chiara, G., Dahlgren, P., Dee, D., Diamantakis, M., Dragani, R., Flemming, J., Forbes, R., Fuentes, M., Geer, A., Haimberger, L., Healy, S., Hogan, R. J., Hólm, E., Janisková, M., Keeley, S., Laloyaux, P., Lopez, P., Lupu, C., Radnoti, G., de Rosnay, P., Rozum, I., Vamborg, F., Villaume, S., and Thépaut, J.-N.: The ERA5 global reanalysis, Quarterly Journal of the Royal Meteorological Society, 146, 1999–2049, https://doi.org/https://doi.org/10.1002/qj.3803, 2020.

Hilton, F., Armante, R., August, T., Barnet, C., Bouchard, A., Camy-Peyret, C., Capelle, V., Clarisse, L., Clerbaux, C., Coheur, P.-F., Collard, A., Crevoisier, C., Dufour, G., Edwards, D., Faijan, F., Fourrié, N., Gambacorta, A., Goldberg, M., Guidard, V., Hurtmans, D., Illingworth, S., Jacquinet-Husson, N., Kerzenmacher, T., Klaes, D., Lavanant, L., Masiello, G., Matricardi, M., McNally, A., Newman, S., Pavelin, E., Payan, S., Péquignot, E., Peyridieu, S., Phulpin, T., Remedios, J., Schlüssel, P., Serio, C., Strow, L., Stubenrauch, C., Taylor, J., Tobin, D., Wolf, W., and Zhou, D.: Hyperspectral Earth Observation from IASI: Five Years of Accomplishments, Bulletin of the American Meteorological Society, 93, 347–370, https://doi.org/10.1175/bams-d-11-00027.1, 2012.

Huang, X., Chen, X., Zhou, D. K., and Liu, X.: An Observationally Based Global Band-by-Band Surface Emissivity Dataset for Climate and Weather Simulations, Journal of the Atmospheric Sciences, 73, 3541 – 3555, https://doi.org/10.1175/JAS-D-15-0355.1, 2016.

IPCC: Climate Change 2021: The Physical Science Basis. Contribution of Working Group I to the Sixth Assessment Report of the Intergovernmental Panel on Climate Change, Cambridge University Press, 2021.

Koroleva, A. O., Odintsova, T. A., Tretyakov, M. Y., Pirali, O., and Campargue, A.: The foreign-continuum absorption of water vapour in the far-infrared (50–500 cm-1), Journal of Quantitative Spectroscopy and Radiative Transfer, 261, 107 486, https://doi.org/https://doi.org/10.1016/j.jqsrt.2020.107486, 2021.

Liou, K. and Yang, P.: Light scattering by ice crystals : fundamentals and applications, Cambridge University Press, Cambridge, 2016.

Liuzzi, G., Masiello, G., Serio, C., Palchetti, L., and Bianchini, G.: Validation of H2O continuum absorption models in the wave number range 180–600 cm−1 with atmospheric emitted spectral radiance measured at the Antarctica Dome-C site, Opt. Express, 22, 16 784–16 801, https://doi.org/10.1364/OE.22.016784, 2014.

Maestri, T., Arosio, C., Rizzi, R., Palchetti, L., Bianchini, G., and Del Guasta, M.: Antarctic Ice Cloud Identification and Properties Using Downwelling Spectral Radiance From 100 to 1,400 cm-1, Journal of Geophysical Research: Atmospheres, 124, 4761–4781, https://doi.org/https://doi.org/10.1029/2018JD029205, 2019a.

Maestri, T., Cossich, W., and Sbrolli, I.: Cloud identification and classification from high spectral resolution data in the far infrared and mid-infrared, Atmospheric Measurement Techniques, 12, 3521–3540, https://doi.org/10.5194/amt-12-3521-2019, 2019b.

Magurno, D., Cossich, W., Maestri, T., Bantges, R., Brindley, H., Fox, S., Harlow, C., Murray, J., Pickering, J., Warwick, L., and Oetjen, H.: Cirrus Cloud Identification from Airborne Far-Infrared and Mid-Infrared Spectra, Remote Sensing, 12, https://doi.org/10.3390/rs12132097, 2020.

Martin, G. M., Johnson, D. W., and Spice, A.: The Measurement and Parameterization of Effective Radius of Droplets in Warm Stratocumulus Clouds, Journal of Atmospheric Sciences, 51, 1823 – 1842, https://doi.org/10.1175/1520-0469(1994)051<1823:TMAPOE>2.0.CO;2, 1994.

Martinazzo, M., Magurno, D., Cossich, W., Serio, C., Masiello, G., and Maestri, T.: Assessment of the accuracy of scaling methods for radiance simulations at far and mid infrared wavelengths, Journal of Quantitative Spectroscopy and Radiative Transfer, 271, 107 739, https://doi.org/https://doi.org/10.1016/j.jqsrt.2021.107739, 2021.

Masiello, G. and Serio, C.: Simultaneous physical retrieval of surface emissivity spectrum and atmospheric parameters from infrared atmospheric sounder interferometer spectral radiances, Appl. Opt., 52, 2428–2446, https://doi.org/10.1364/AO.52.002428, 2013.

Mlawer, E. J., Turner, D. D., Paine, S. N., Palchetti, L., Bianchini, G., Payne, V. H., Cady-Pereira, K. E., Pernak, R. L., Alvarado, M. J., Gombos, D., Delamere, J. S., Mlynczak, M. G., and Mast, J. C.: Analysis of Water Vapor Absorption in the Far-Infrared and Submillimeter Regions Using Surface Radiometric Measurements From Extremely Dry Locations, Journal of Geophysical Research: Atmospheres, 124, 8134–8160, https://doi.org/https://doi.org/10.1029/2018JD029508, 2019.

OpenMP Architecture Review Board: OpenMP Application Program Interface Version 5.0, https://www.openmp.org/wp-content/uploads/OpenMP-API-Specification-5.0.pdf, 2018.

Palchetti, L., Bianchini, G., Natale, G. D., and Guasta, M. D.: Far-Infrared Radiative Properties of Water Vapor and Clouds in Antarctica, Bulletin of the American Meteorological Society, 96, 1505 – 1518, https://doi.org/10.1175/BAMS-D-13-00286.1, 2015.

Palchetti, L., Di Natale, G., and Bianchini, G.: Remote sensing of cirrus cloud microphysical properties using spectral measurements over the full range of their thermal emission, Journal of Geophysical Research: Atmospheres, 121, 10,804–10,819, https://doi.org/https://doi.org/10.1002/2016JD025162, 2016.

Palchetti, L., Brindley, H., Bantges, R., Buehler, S. A., Camy-Peyret, C., Carli, B., Cortesi, U., Del Bianco, S., Di Natale, G., Dinelli, B. M., Feldman, D., Huang, X. L., C. Labonnote, L., Libois, Q., Maestri, T., Mlynczak, M. G., Murray, J. E., Oetjen, H., Ridolfi, M., Riese, M., Russell, J., Saunders, R., and Serio, C.: FORUM: unique far-infrared satellite observations to better understand how Earth radiates energy to space, Bulletin of the American Meteorological Society, pp. 1–52, https://doi.org/10.1175/BAMS-D-19-0322.1, 2020.

Paul, M., Aires, F., Prigent, C., Trigo, I. F., and Bernardo, F.: An innovative physical scheme to retrieve simultaneously surface temperature and emissivities using high spectral infrared observations from IASI, Journal of Geophysical Research: Atmospheres, 117, https://doi.org/https://doi.org/10.1029/2011JD017296, 2012.

Peña, O. and Pal, U.: Scattering of electromagnetic radiation by a multilayered sphere, Computer Physics Communications, 180, 2348–2354, https://doi.org/10.1016/j.cpc.2009.07.010, 2009.

Remedios, J. J., Leigh, R. J., Waterfall, A. M., Moore, D. P., Sembhi, H., Parkes, I., Greenhough, J., Chipperfield, M. P., and Hauglustaine, D.: MIPAS reference atmospheres and comparisons to V4.61/V4.62 MIPAS level 2 geophysical data sets, Atmospheric Chemistry and Physics Discussions, 7, 9973–10 017, https://doi.org/10.5194/acpd-7-9973-2007, 2007.

Ridolfi, M. and Sgheri, L.: Iterative approach to self-adapting and altitude-dependent regularization for atmospheric profile retrievals, Opt. Express, 19, 26 696–26 709, https://doi.org/10.1364/OE.19.026696, 2011.

Ridolfi, M., Del Bianco, S., Di Roma, A., Castelli, E., Belotti, C., Dandini, P., Di Natale, G., Dinelli, B. M., C.-Labonnote, L., and Palchetti, L.: FORUM Earth Explorer 9: Characteristics of Level 2 Products and Synergies with IASI-NG, Remote Sensing, 12, https://doi.org/10.3390/rs12091496, 2020.

Rodgers, C. D.: Inverse Methods for Atmospheric Sounding, WORLD SCIENTIFIC, https://doi.org/10.1142/3171, 2000.

Saito, M., Yang, P., Huang, X., Brindley, H. E., Mlynczak, M. G., and Kahn, B. H.: Spaceborne Middle- and Far-Infrared Observations Improving Nighttime Ice Cloud Property Retrievals, Geophysical Research Letters, 47, https://doi.org/10.1029/2020gl087491, 2020.

Salisbury, J. W. and D'Aria, D. M.: Emissivity of terrestrial materials in the 8–14 μm atmospheric window, Remote Sensing of Environment, 42, 83–106, https://doi.org/https://doi.org/10.1016/0034-4257(92)90092-X, 1992.

Serio, C., Masiello, G., Esposito, F., Girolamo, P. D., Iorio, T. D., Palchetti, L., Bianchini, G., Muscari, G., Pavese, G., Rizzi, R., Carli, B., and Cuomo, V.: Retrieval of foreign-broadened water vapor continuum coefficients from emitted spectral radiance in the H_2O rotational band from 240 to 590 cmˆ-1, Optics Express, 16, 15 816, https://doi.org/10.1364/oe.16.015816, 2008.

Sgheri, L. and Castelli, E.: Speeding up the DISORT solver: mathematical approach and application to radiance simulations of FORUM, in: ESA ATMOS Conference, Salzburg, 2018.

Sgheri, L., Raspollini, P., and Ridolfi, M.: Auto-adaptive Tikhonov regularization of water vapor profiles: application to FORUM measurements, Applicable Analysis, 0, 1–11, https://doi.org/10.1080/00036811.2020.1751825, 2020.

Sinha, A. and Harries, J. E.: Water vapour and greenhouse trapping: The role of far infrared absorption, Geophysical Research Letters, 22, 2147–2150, https://doi.org/10.1029/95gl01891, 1995.

Stengel, M., Stapelberg, S., Sus, O., Schlundt, C., Poulsen, C., Thomas, G., Christensen, M., Carbajal Henken, C., Preusker, R., Fischer, J., Devasthale, A., Willén, U., Karlsson, K.-G., McGarragh, G. R., Proud, S., Povey, A. C., Grainger, R. G., Meirink, J. F., Feofilov, A., Bennartz, R., Bojanowski, J. S., and Hollmann, R.: Cloud property datasets retrieved from AVHRR, MODIS, AATSR and MERIS in the framework of the Cloud_cci project, Earth System Science Data, 9, 881–904, https://doi.org/10.5194/essd-9-881-2017, 2017.

Sun, Z.: Reply to comments by Greg M. McFarquhar on 'Parametrization of effective sizes of cirrus-cloud particles and its verification against observations'. (October B, 1999, 125, 3037–3055), Quarterly Journal of the Royal Meteorological Society, 127, 267–271, https://doi.org/https://doi.org/10.1002/qj.49712757116, 2001.

Sun, Z. and Rikus, L.: Parametrization of effective sizes of cirrus-cloud particles and its verification against observations, Quarterly Journal of the Royal Meteorological Society, 125, 3037–3055, https://doi.org/https://doi.org/10.1002/qj.49712556012, 1999.

Sánchez-Nogales, M.: Earth Observation Mission CFI Software GENERAL SOFTWARE USER MANUAL, DEIMOS, ESA, 2020.

Turner, D. D., Ackerman, S. A., Baum, B. A., Revercomb, H. E., and Yang, P.: Cloud Phase Determination Using Ground-Based AERI Observations at SHEBA, Journal of Applied Meteorology, 42, 701 – 715, https://doi.org/10.1175/1520-0450(2003)042<0701:CPDUGA>2.0.CO;2, 2003.

Veglio, P. and Maestri, T.: Statistics of vertical backscatter profiles of cirrus clouds, Atmospheric Chemistry and Physics, 11, 12 925–12 943, https://doi.org/10.5194/acp-11-12925-2011, 2011.

Wessel, P. and Smith, W. H. F.: A global, self-consistent, hierarchical, high-resolution shoreline database, Journal of Geophysical Research: Solid Earth, 101, 8741–8743, https://doi.org/https://doi.org/10.1029/96JB00104, 1996.

Wielicki, B. A., Young, D. F., Mlynczak, M. G., Thome, K. J., Leroy, S., Corliss, J., Anderson, J. G., Ao, C. O., Bantges, R., Best, F., Bowman, K., Brindley, H., Butler, J. J., Collins, W., Dykema, J. A., Doelling, D. R., Feldman, D. R., Fox, N., Huang, X., Holz, R., Huang, Y., Jin, Z., Jennings, D., Johnson, D. G., Jucks, K., Kato, S., Kirk-Davidoff, D. B., Knuteson, R., Kopp, G., Kratz, D. P., Liu, X., Lukashin, C., Mannucci, A. J., Phojanamongkolkij, N., Pilewskie, P., Ramaswamy, V., Revercomb, H., Rice, J., Roberts, Y., Roithmayr, C. M., Rose, F., Sandford, S., Shirley, E. L., Smith, W. L., Soden, B., Speth, P. W., Sun, W., Taylor, P. C., Tobin, D., and Xiong, X.: Achieving Climate Change Absolute Accuracy in Orbit, Bulletin of the American Meteorological Society, 94, 1519–1539, https://doi.org/10.1175/BAMS-D-12-00149.1, publisher: American Meteorological Society Section: Bulletin of the American Meteorological Society, 2013.

Yang, P., Bi, L., Baum, B. A., Liou, K.-N., Kattawar, G. W., Mishchenko, M. I., and Cole, B.: Spectrally Consistent Scattering, Absorption, and Polarization Properties of Atmospheric Ice Crystals at Wavelengths from 0.2 to 100 µm, Journal of the Atmospheric Sciences, 70, 330 – 347, https://doi.org/10.1175/JAS-D-12-039.1, 2013.